The COG complex interacts directly with Syntaxin 6 and positively regulates endosome-to-TGN retrograde transport

Orly Laufman,[1] WanJin Hong,[2,3] and Sima Lev[1]

[1]Molecular Cell Biology Department, Weizmann Institute of Science, Rehovot 76100, Israel
[2]Institute for Biomedical Research, Xiamen University, Xiamen, Fujian 361005, People's Republic of China
[3]Cancer and Developmental Cell Biology Division, Institute of Molecular and Cell Biology, Singapore 138673

The conserved oligomeric Golgi (COG) complex has been implicated in the regulation of endosome to trans-Golgi network (TGN) retrograde trafficking in both yeast and mammals. However, the exact mechanisms by which it regulates this transport route remain largely unknown. In this paper, we show that COG interacts directly with the target membrane SNARE (t-SNARE) Syntaxin 6 via the Cog6 subunit. In Cog6-depleted cells, the steady-state level of Syntaxin 6 was markedly reduced, and concomitantly, endosome-to-TGN retrograde traffic was significantly attenuated. Cog6 knockdown also affected the steady-state levels and/or subcellular distributions of Syntaxin 16, Vti1a, and VAMP4 and impaired the assembly of the Syntaxin 6–Syntaxin16–Vti1a–VAMP4 SNARE complex. Remarkably, overexpression of VAMP4, but not of Syntaxin 6, bypassed the requirement for COG and restored endosome-to-TGN trafficking in Cog6-depleted cells. These results suggest that COG directly interacts with specific t-SNAREs and positively regulates SNARE complex assembly, thereby affecting their associated trafficking steps.

Introduction

Retrograde transport from the endosomal compartments (late and early/recycling endosomes) to the TGN is implicated in diverse cellular, developmental, and pathological processes (Johannes and Popoff, 2008). It is required for the transport of lysosomal acid hydrolases and the recycling of various membrane proteins and signaling receptors. It is also involved in the transport of certain processing peptidases, SNAREs, and transporters as well as bacteria and plant toxins (Bonifacino and Rojas, 2006). The delivery of Shiga toxin, cholera toxin, and ricin, for example, is dependent on this trafficking route. Similarly, the recycling of the mannose 6–phosphate receptors (MPRs), the transmembrane peptidase furin, the TGN resident protein TGN38/46, the t-SNARE Stx6 (Syntaxin 6), and the v-SNARE VAMP4 also requires this transport route (Ghosh et al., 2003; Bonifacino and Rojas, 2006; Tran et al., 2007; Johannes and Popoff, 2008).

Numerous studies have shown that several distinct pathways mediate endosome-to-TGN transport (Sannerud et al., 2003; Pfeffer, 2009). These pathways use different Rab GTPases, tethering factors, and SNARE complexes. Transport from the late endosomes to the TGN is regulated by the Stx10–Stx16–Vti1a–VAMP3 SNARE complex and requires the Rab9 GTPase (Ganley et al., 2008), whereas transport from early/recycling endosomes to the TGN is mediated by the Stx6–Stx16–Vti1a–VAMP4 SNARE complex and requires the Rab6A/Rab11 GTPases (Mallard et al., 2002). The Stx5–GS28–Ykt6–GS15 SNARE complex, which regulates intra-Golgi retrograde transport, has also been implicated in retrograde transport from early/recycling endosomes to the Golgi complex (Mallard et al., 2002; Tai et al., 2004; Amessou et al., 2007). These SNARE complexes cooperate with multiple tethering factors, including the elongated coiled-coil tethers of the Golgin family: Golgin 97, Golgin 245, GCC185, and GCC88. It has been shown that Golgin 97, Golgin 245, and GCC185 are required

Correspondence to Sima Lev: sima.lev@weizmann.ac.il

Abbreviations used in this paper: BFA, brefeldin A; CI-MPR, cation-independent MPR; COG, conserved oligomeric Golgi; GARP, Golgi-associated retrograde protein; KD, knockdown; KDELR, KDEL receptor; MPR, mannose 6–phosphate receptor; MTC, multisubunit tethering complex; NEM, *N*-ethylmaleimide; shRNA, short hairpin RNA; STx-B, Shiga toxin B subunit.

The Rockefeller University Press $30.00
J. Cell Biol. Vol. 194 No. 3 459–472
www.jcb.org/cgi/doi/10.1083/jcb.201102045

for efficient retrograde trafficking of the Shiga toxin B subunit (STx-B), whereas GCC88 is required for the retrieval of TGN38/46 to the TGN (Luke et al., 2003; Yoshino et al., 2005; Lieu et al., 2007). The multisubunit tethering complex (MTC) Golgi-associated retrograde transport protein (GARP) complex is also essential for retrograde transport of STx-B as well as for the retrieval of TGN38/46 and the cation-independent (CI) MPR (Pérez-Victoria et al., 2008). This MTC is involved in the assembly of the Stx6–Stx16–Vti1a–VAMP4 SNARE complex, thereby regulating the fusion of endosome-derived vesicles with the TGN membrane (Pérez-Victoria and Bonifacino, 2009). The conserved oligomeric Golgi (COG) complex has also been implicated in endosome-to-TGN retrograde transport.

COG is an evolutionally conserved Golgi-associated tethering complex composed of eight subunits (Cog1–Cog8), which can be divided into two structurally and functionally distinct subcomplexes, lobe A (Cog1–4) and lobe B (Cog5–8) (Walter et al., 1998; Whyte and Munro, 2001; Ram et al., 2002; Ungar et al., 2002; Loh and Hong, 2004). Subunits of the first lobe are essential for cell growth in yeast and, therefore, are considered as essential components of the complex (Wuestehube et al., 1996; VanRheenen et al., 1998; Whyte and Munro, 2001). Mutations in the different COG subunits severely distress the Golgi glycosylation machinery and result in substantial alterations in global cell surface glycoconjugates (Reddy and Krieger, 1989; Wuestehube et al., 1996; Chatterton et al., 1999; Oka et al., 2005; Shestakova et al., 2006). The profound effect of COG on the Golgi glycosylation machinery and its association with congenital disorders of glycosylation in humans (Wu et al., 2004; Foulquier et al., 2006, 2007; Kranz et al., 2007; Zeevaert et al., 2008) suggest that COG is involved in the transport, retention, and/or retrieval of Golgi glycosylation enzymes. Indeed, genetic and biochemical studies in yeast and mammalian cells suggest that COG functions as a tethering factor for vesicles that recycle within the Golgi apparatus, thereby regulating intra-Golgi retrograde transport and, consequently, the proper localization of Golgi glycosylation enzymes (Walter et al., 1998; Suvorova et al., 2001, 2002; Bruinsma et al., 2004; Ungar et al., 2006).

Like other MTCs, COG is thought to bridge the transport vesicle with its target membrane through binding of Rab GTPases, SNAREs, and/or vesicle coats. Consistent with this mode of action, COG was found to interact directly with the small GTPase Ypt1p (Rab1), with the γ-COP subunit of the COPI coat complex, and with the Golgi t-SNARE Sed5/Stx5 (Suvorova et al., 2002; Shestakova et al., 2007). COG interacts with Stx5 via its Cog4 subunit and appears to stabilize the intra-Golgi Stx5–GS28–Ykt6–GS15 SNARE complex (Shestakova et al., 2007; Laufman et al., 2009). Previously, we found that COG also interacts directly with the SM (Sec1/Munc18-like) protein Sly1 via its Cog4 subunit and that the Cog4–Sly1 interaction is required for Stx5–GS28–Ykt6–GS15 SNARE complex assembly and, consequently, for retrograde transport from the Golgi complex (Laufman et al., 2009).

In addition to its key role in intra-Golgi retrograde transport (Suvorova et al., 2002; Bruinsma et al., 2004), COG was also proposed to tether vesicles that recycle to the Golgi complex from the endosomal compartments (VanRheenen et al., 1999). Mutations in the yeast COG complex impair the sorting of vacuolar hydrolase carboxypeptidase Y and the retrieval of the v-SNARE Snc1p from the endosomal system back to the Golgi complex (Wuestehube et al., 1996; Spelbrink and Nothwehr, 1999; Whyte and Munro, 2001). Likewise, depletion of certain COG subunits by RNAi in mammalian cells impairs endosome-to-TGN retrograde transport of STx-B and of subtilase cytotoxin (Zolov and Lupashin, 2005; Sun et al., 2007; Smith et al., 2009). These observations suggest that COG is involved in both intra-Golgi and endosome to Golgi retrograde transport. However, it remains unclear whether COG directly regulates endosome-to-TGN traffic or indirectly influences this pathway as a result of its major effect on intra-Golgi retrograde transport.

Here, we show that COG directly and positively regulates endosome-to-TGN retrograde transport by specific and direct interaction with the endosome-to-TGN fusion machinery. We found that COG interacts directly with the t-SNARE Stx6 via its Cog6 subunit. In Cog6-depleted cells, endosome-to-TGN retrograde transport of STx-B and TGN38 is markedly attenuated, and concomitantly, the steady-state distribution of TGN46, CI-MPR, and γ-adaptin is impaired. Cog6 knockdown (KD) also affects the steady-state distribution of Stx16, Vti1a, and VAMP4 and enhances their steady-state levels. In contrast, the steady-state level of the Stx6 protein is substantially reduced in Cog6-depleted cells, and its TGN localization is apparently abolished. Yet, overexpression of Stx6 fails to restore endosome-to-TGN transport in Cog6-depleted cells. Overexpression of the v-SNARE VAMP4, however, bypasses the requirement for COG and restores both the TGN localization of Stx6 and endosome-to-TGN retrograde transport in Cog6-depleted cells. These results suggest that COG positively regulates both the stability and the recycling of Stx6, thereby affecting SNARE complex assembly at the TGN and, consequently, endosome-to-TGN retrograde trafficking.

Results

Endosome-to-TGN retrograde transport is attenuated in Cog6-depleted cells

A previous study has shown that KD of the Cog3 subunit in mammalian cells substantially inhibited retrograde transport of STx-B to the Golgi complex (Zolov and Lupashin, 2005). To examine the influence of other COG subunits on the retrograde transport of STx-B, we depleted the expression of the Cog6 subunit in HeLa cells by short hairpin RNAs (shRNAs; Fig. S1 A). As shown, KD of Cog6 distinctly affected the steady-state levels of the different COG subunits (Fig. S1 B) but had minor effects on both the Golgi morphology and the Golgi localization of the first lobe's subunits (Cog1–4; Fig. S1 C). However, it almost completely abrogated the Golgi localization of Cog5 and Cog7 subunits and markedly attenuated both retrograde transport from the Golgi complex (Fig. S1, D and E) and retrograde transport of STx-B to the TGN. As shown in Fig. 1 A, the binding of STx-B to the cell surface at 4°C was unaffected by Cog6 depletion. However, 45 min after shifting the temperature to 37°C, STx-B was localized to the Golgi complex in the majority of the control cells (98%; $n = 200$) but could hardly

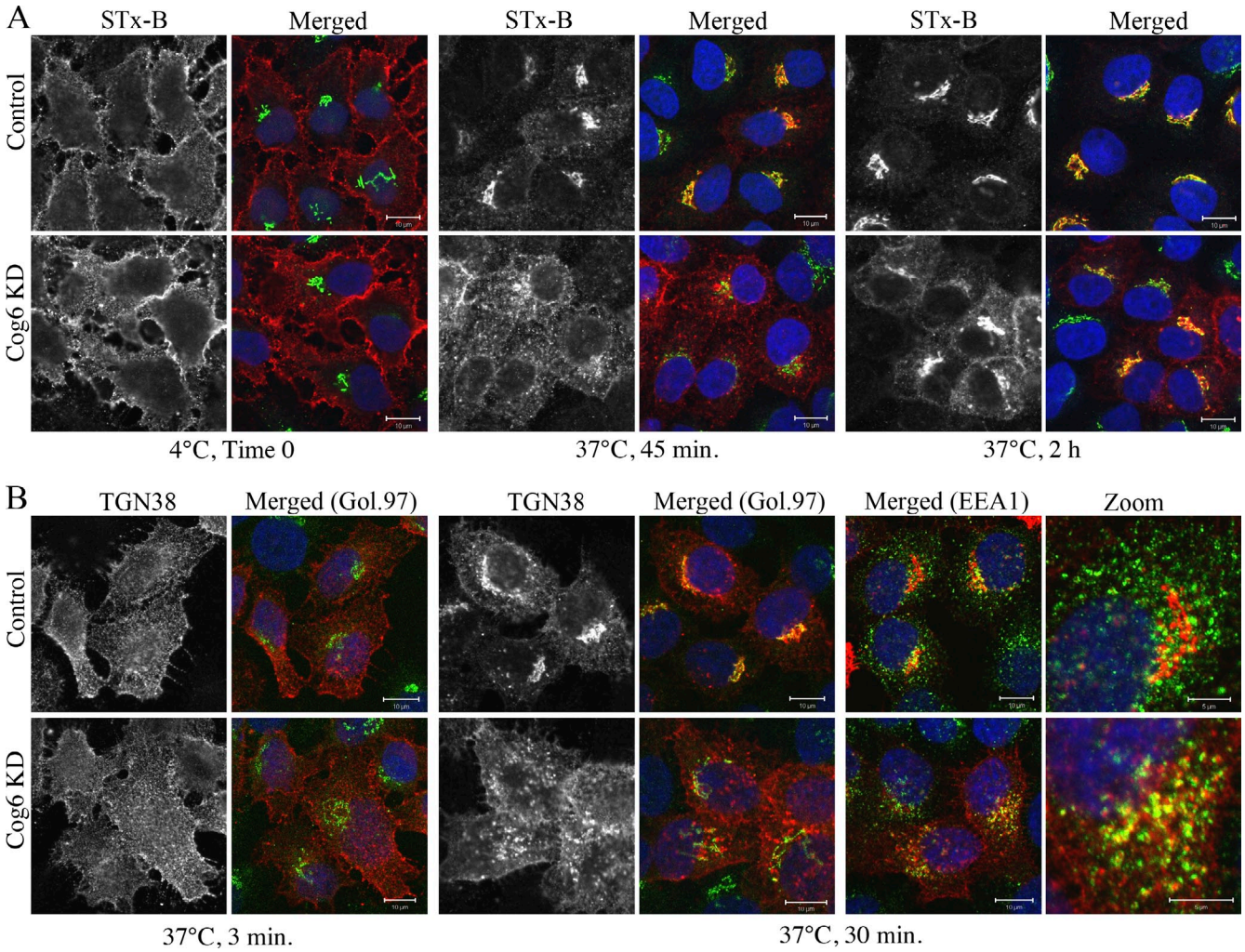

Figure 1. **Endosome-to-TGN retrograde transport of STx-B and TGN38 is attenuated in Cog6-depleted cells.** (A) Endosome-to-TGN transport of STx-B. Control (pSUPER-puro) and Cog6-depleted (KD) HeLa cells were incubated with recombinant purified His-tagged STx-B (1 µg/ml) for 30 min at 4°C and either fixed (Time 0) or transferred to 37°C for the indicated time periods. The cells were then fixed, double immunostained with anti-His (red) and anti–Golgin 97 (Gol.97; green) antibodies, and analyzed by confocal microscopy. Shown are representative confocal images at the indicated time points. (B) Endosome-to-TGN transport of HA-tagged TGN38. Control and Cog6-depleted HeLa cells expressing HA-TGN38 were incubated at 37°C with the anti-HA monoclonal antibody for various time periods (Fig. S2 B). The localizations of TGN38-HA (red) and Golgin 97 (green) were determined by immunostaining and confocal microscopy analysis. Shown are representative confocal images of control and Cog6-depleted cells at 3 and 30 min of antibody uptake. Bars: (A and B, main images) 10 µm; (B, zoom) 5 µm.

be detected in the Golgi of Cog6-depleted cells (5%; $n = 200$). Instead, it was predominantly distributed in various punctate cytosolic structures (Fig. 1 A), which displayed weak colocalization with the TGN marker Golgin 97 (11 ± 7% in Cog6-depleted cells as compared with 66 ± 12% in control cells; $n = 30$). These structures were partially colocalized with the early endosomal marker EEA1 (Fig. S2 A), consistent with the transport of STx-B from the early/recycling endosomes to the TGN (Mallard et al., 1998). At 2 h after internalization, STx-B was localized mainly to the TGN of Cog6-depleted cells but could also be detected in punctate structures throughout the cytosol, suggesting that depletion of Cog6 markedly attenuates endosome-to-TGN trafficking of STx-B.

To further assess the effect of Cog6 KD on endosome-to-TGN transport, we examined the trafficking of TGN38 from the cell surface to the TGN using an antibody uptake assay (Reaves et al., 1993). TGN38/46 is a resident TGN protein that constitutively cycles between the TGN and the plasma membrane via early/recycling endosomes (Ghosh et al., 1998). Control and Cog6-depleted HeLa cells expressing a HA-tagged TGN38 were incubated with the anti-HA antibody for various periods of time, fixed, and double immunostained for TGN38-HA and either the TGN marker Golgin 97 or the early endosomal marker EEA1. As shown, TGN38-HA rapidly internalized into the cells and reached the Golgi complex of the control cells within ∼15–30 min (Figs. 1 B and S2 B). At 30 min of antibody uptake, the colocalization between TGN38 and Golgin 97 reached to 60 ± 15% in the control cells ($n = 30$). In contrast, only 15 ± 10% of TGN38 fluorescence was colocalized with Golgin 97 in Cog6-depleted cells ($n = 30$), and instead, extensive colocalization between TGN38 and EEA1 was detected (Fig. 1 B). These results suggest that the COG complex is essential for retrograde transport of both STx-B and TGN38/46 from early/recycling endosomes to the TGN.

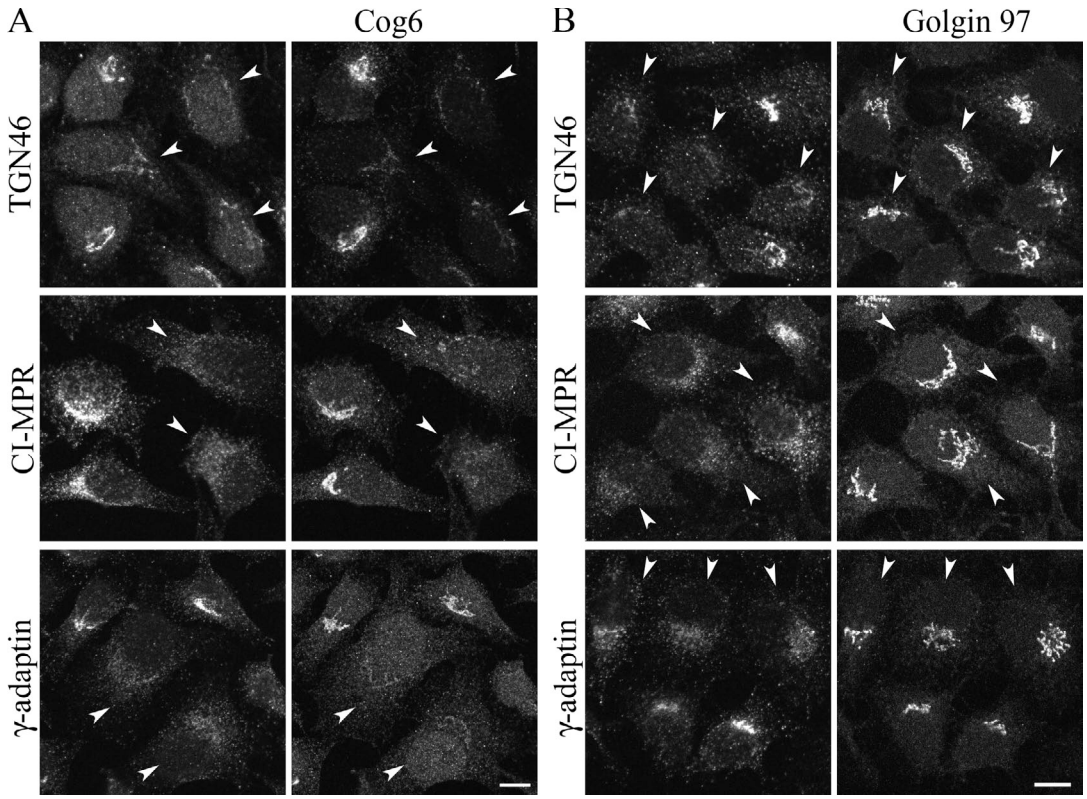

Figure 2. **Depletion of Cog6 impairs the Golgi localization of TGN46, CI-MPR, and γ-adaptin.** (A and B) HeLa cells were transiently transfected with a Cog6 shRNA construct (A) or cotransfected with the Cog6 shRNA construct together with a vector encoding EGFP (B). 72 h later, the cells were fixed and double immunostained with an antibody against TGN46, CI-MPR, or γ-adaptin and either the anti-Cog6 antibody (A) or anti–Golgin 97 antibody (B). The TGN localization of TGN46, CI-MPR, or γ-adaptin was determined by colocalization with Golgin 97 (B). Cog6-depleted cells, which are marked by arrowheads, were identified either by immunostaining with the anti-Cog6 antibody (A) or by EGFP expression (B). Bars, 10 µm.

To confirm these transport assays results, we examined the steady-state distribution of various endogenous proteins that recycle between the early/recycling endosomes and the TGN, including the CI-MPR, TGN46, and γ-adaptin, a component of the AP-1 complex, which is required for endosome-to-TGN transport of MPRs (Meyer et al., 2000). As shown in Fig. 2, CI-MPR, TGN46, and γ-adaptin predominantly localized to the TGN of the control cells, consistent with previous studies (Reaves et al., 1993; Ghosh et al., 1998; Saint-Pol et al., 2004). Their TGN localization, however, was markedly reduced in Cog6-depleted cells, and instead, they were predominantly seen in faint cytosolic structures. These results suggest that the trafficking of endogenous CI-MPR, TGN46, and γ-adaptin from early/recycling endosomes to the Golgi apparatus is perturbed in the absence of an intact COG complex, and consequently, their Golgi localization is affected.

Depletion of Cog6 affects the TGN localization of Stx6 and its colocalization with Stx16, Vti1a, and VAMP4

The profound effect of Cog6 KD on the steady-state distribution of CI-MPR, TGN46, and γ-adaptin (Fig. 2) led us to examine its influence on the subcellular distributions of SNAREs that regulate endosome-to-TGN trafficking. The localization experiments shown in Fig. 3 A demonstrate the striking effect of Cog6 KD on the steady-state distribution of Stx6. In control cells, Stx6 was localized mainly in the TGN, consistent with previous studies (Bock et al., 1997; Klumperman et al., 1998; Wendler and Tooze, 2001). In Cog6-depleted cells, however, Stx6 lost its characteristic TGN localization and was observed in very faint cytosolic structures that could hardly be detected. These structures failed to colocalize with the early endosomal marker EEA1, suggesting that depletion of Cog6 affects the recycling of Stx6 to the TGN.

Next, we examined the effect of Cog6 KD on the steady-state distribution of other SNAREs of the Stx6–Stx16–Vti1a–VAMP4 SNARE complex. As shown in Fig. 3 B, the Golgi localization of Stx16 was markedly reduced in Cog6-depleted cells as compared with control HeLa cells. Yet, a residual Golgi staining of Stx16 could be observed. Depletion of Cog6 also impaired the Golgi localization of VAMP4, and it was mainly detected in various cytosolic structures. In contrast, Vti1a was localized to the Golgi of Cog6-depleted cells, similar to its location in control cells. Nevertheless, Vti1a as well as Stx16 and VAMP4 lost their colocalization with Stx6, implying that depletion of Cog6 impairs the assembly of the Stx6–Stx16–Vti1a–VAMP4 SNARE complex. Collectively, these results suggest that Cog6 KD strikingly affects the steady-state distribution of Stx6 and also influences the distribution of its associated SNAREs. It is worth mentioning that Cog6 KD had no detectable effects on the Golgi localization of either Stx5 or GS28 (Fig. S3). Yet, it abrogated the colocalization of GS15 with

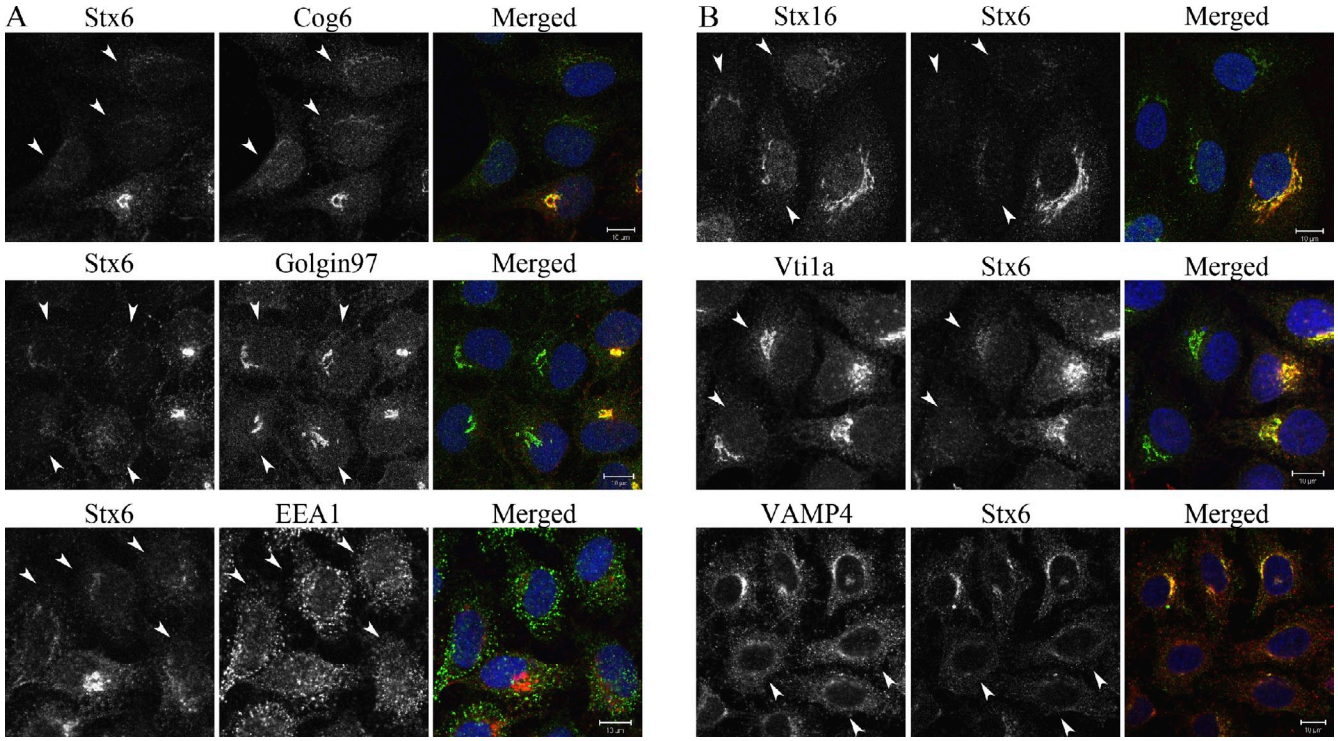

Figure 3. **The TGN localization of Stx6 and its colocalization with Stx16, Vti1a, and VAMP4 are abolished in Cog6-depleted cells.** (A) The TGN localization of Stx6 (red) in Cog6-depleted cells (marked by arrowheads) was determined by colocalization with Golgin 97 (green; middle), whereas colocalization with EAA1 (green) was used to assess its localization on early endosomes (bottom). (B) The colocalization of Stx6 with Stx16 (green), Vti1a (green), or VAMP4 (red) was determined in control and Cog6-depleted (marked by arrowheads) cells. Bars, 10 µm.

Stx5 (Fig. S3), consistent with the established role of COG in Stx5–GS28–Ykt6–GS15 SNARE complex assembly (Shestakova et al., 2007; Laufman et al., 2009).

Depletion of Cog6 affects the steady-state level and distribution of Stx6, its associated SNAREs, and SNARE complex assembly

To further confirm the immunostaining results shown in Fig. 3, we assessed the steady-state levels and the subcellular distribution of Stx6, Stx16, Vti1a, and VAMP4 by Western blotting (Fig. 4 A) and by subcellular fractionation (Fig. 4 C), respectively. As shown in Fig. 4 A, a substantial decrease (∼50%) in the steady-state level of Stx6 was observed in Cog6-depleted cells, which is consistent with the faint immunostaining results (Fig. 3 A). In contrast, the steady-state levels of Vti1a, Stx16, and VAMP4 increased by ∼40–50%. Interestingly, the steady-state level of the v-SNARE GS15 was also increased in Cog6-depleted cells, whereas the levels of its associated t-SNAREs, Stx5, GS28, and Ykt6, were unaffected by Cog6 depletion (Fig. 4 B). These results suggest that depletion of Cog6 distinctly affects the steady-state levels of SNAREs of the Stx6–Stx16–Vti1a–VAMP4 SNARE complex.

We next examined the subcellular distribution of these SNAREs by cell fractionation applying differential centrifugation. Cell homogenates were fractionated into heavy membranes, light membranes, and cytosol and analyzed by Western blotting and densitometry for SNARE distribution. As seen in Fig. 4 C, Stx6 was distributed almost equally between the heavy and light membrane fractions of the control cells. In contrast, it was highly enriched in the light membrane fraction (∼70%), which contains various vesicles, in Cog6-depleted cells. Its association with the heavy membrane fraction, containing the Golgi membranes, could hardly be detected in Cog6-depleted cells, consistent with the immunostaining results (Fig. 3 A) and its overall reduced steady-state level (Fig. 4 A). The distribution of Stx16, Vti1a, and VAMP4 was also affected by Cog6 KD, and these three SNARE proteins were enriched in the light membrane fraction compared with control cells (Fig. 4 C). A high level of Vti1a was also detected in the heavy membrane fraction of Cog6-depleted cells, which is consistent with its Golgi association shown in Fig. 3 B and its increased steady-state level (Fig. 4 A). Collectively, these results show that KD of Cog6 enhances the association of all these SNAREs with vesicles or other light membranes but selectively reduces the steady-state level of Stx6.

This marked effect of Cog6 depletion on SNARE distribution could affect SNAREpin assembly and, consequently, endosome-to-TGN retrograde transport. We therefore examined the effect of Cog6 KD on SNARE complex assembly by applying a coimmunoprecipitation assay. Control and Cog6-depleted HeLa cells were treated with *N*-ethylmaleimide (NEM), which inhibits NSF, thereby preventing SNARE complex disassembly. Cells were then solubilized and subjected to immunoprecipitation with the anti-Vti1a antibody. The association of Vti1a with Stx6, Stx16, and VAMP4 was determined by immunoblotting with the corresponding antibodies. As shown in Fig. 4 D, the four SNARE proteins could be detected in Vti1a immunocomplexes

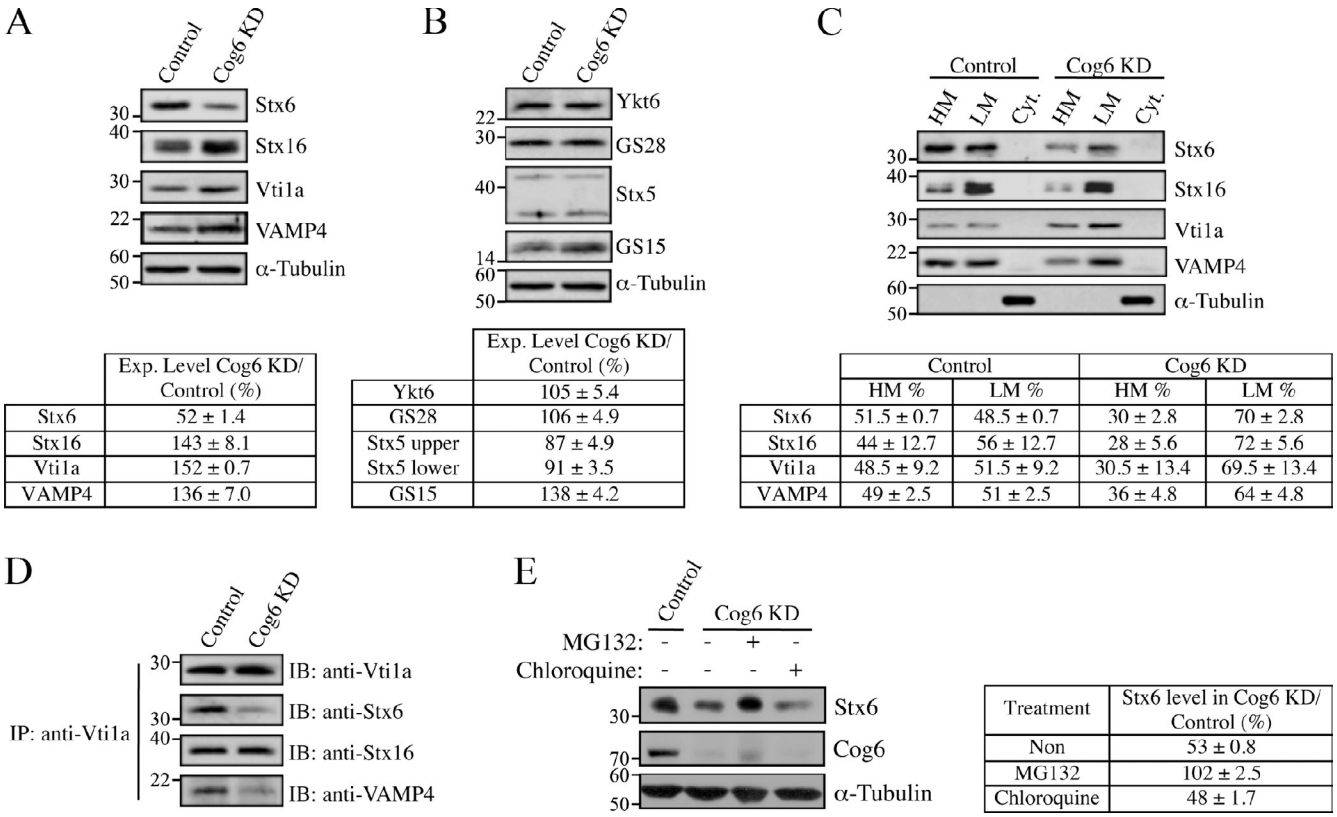

	Exp. Level Cog6 KD/ Control (%)
Stx6	52 ± 1.4
Stx16	143 ± 8.1
Vti1a	152 ± 0.7
VAMP4	136 ± 7.0

	Exp. Level Cog6 KD/ Control (%)
Ykt6	105 ± 5.4
GS28	106 ± 4.9
Stx5 upper	87 ± 4.9
Stx5 lower	91 ± 3.5
GS15	138 ± 4.2

	Control		Cog6 KD	
	HM %	LM %	HM %	LM %
Stx6	51.5 ± 0.7	48.5 ± 0.7	30 ± 2.8	70 ± 2.8
Stx16	44 ± 12.7	56 ± 12.7	28 ± 5.6	72 ± 5.6
Vti1a	48.5 ± 9.2	51.5 ± 9.2	30.5 ± 13.4	69.5 ± 13.4
VAMP4	49 ± 2.5	51 ± 2.5	36 ± 4.8	64 ± 4.8

Treatment	Stx6 level in Cog6 KD/ Control (%)
Non	53 ± 0.8
MG132	102 ± 2.5
Chloroquine	48 ± 1.7

Figure 4. **Steady-state levels, subcellular distribution, and SNARE complex assembly of Stx6, Stx16, Vti1a, and VAMP4 in Cog6-depleted cells.** (A and B) The steady-state levels of SNAREs of either the Stx6–Stx16–Vti1a–VAMP4 SNARE complex (A) or the Stx5–GS28–Ykt6–GS15 SNARE complex (B) were determined by Western blotting of total cell lysates of control (pSUPER-puro) and Cog6-depleted HeLa cells using the corresponding antibodies. Densitometric analysis of the Western blot signals was used to estimate the relative level of each SNARE in Cog6-depleted cells as compared with the control HeLa cells. The mean values ± SD of three independent experiments are shown in the table. (C) The subcellular distribution of Stx6 and its associated SNAREs was determined by cell fractionation followed by Western blot analysis using the indicated antibodies. The distribution of each SNARE between the cytosol (Cyt.), heavy membrane (HM), and light membrane (LM) fractions in the control and Cog6-depleted HeLa cells is shown at the top. The relative distribution of each SNARE between the heavy and light membrane fractions was calculated from three independent experiments, and mean values ± SD are shown at the bottom. (D) SNARE complex assembly is impaired in Cog6-depleted cells. Control and Cog6-depleted HeLa cells were pretreated with NEM, solubilized, and subjected to immunoprecipitation (IP) with the anti-Vti1a antibody. The presence of Stx6, Stx16, and VAMP4 in the Vti1a immunocomplex was determined by immunoblotting (IB) using the corresponding antibodies. (E) Stx6 is degraded by the proteasome in Cog6-depleted cells. Cog6-depleted HeLa cells were treated with either the proteasome inhibitor MG132 (1 µM) or the lysosomal inhibitor chloroquine (10 µM) for 24 h. The level of Stx6 in control cells and in the inhibitor-treated Cog6-depleted cells was determined by Western blotting using the anti-Stx6 antibody. The table shows mean values ± SD. Molecular masses are indicated in kilodaltons. Exp., expression.

of control cells, suggesting that SNARE complexes are assembled and can be isolated by this method. However, Stx6 and VAMP4 could hardly be detected in the Vti1a immunocomplexes of Cog6-depleted cells, suggesting that KD of Cog6 markedly affects the steady-state level of Stx6 and, consequently, impairs the assembly of the Stx6–Stx16–Vti1a–VAMP4 SNARE complex.

It was previously shown that depletion of different COG subunits affects the steady-state levels of a subset of type II Golgi membrane proteins known as GEARs, including the Golgi SNAREs GS28 and GS15. These GEARS (GS28, GS15, GPP130, CASP, giantin, and Golgin 84) are mislocalized in COG-deficient cells, and some are abnormally degraded by the proteasome (Oka et al., 2004, 2005). The marked effect of Cog6 KD on the steady-state level of Stx6 implies that it may also undergo abnormal proteasomal degradation. To explore this possibility, Cog6-depleted cells were treated with either the proteasome inhibitor MG132 or the lysosomal inhibitor chloroquine, and the level of Stx6 was examined by Western blotting. As shown, MG132 restored the level of Stx6 in Cog6-depleted cells, suggesting that Stx6 is abnormally degraded by the proteasome in the absence of Cog6 subunit (Fig. 4 E). Interestingly, KD of either the Cog4 or Cog8 subunits had no marked effect on the steady-state level of Stx6 (Fig. S4 A). Likewise, depletion of Cog6 had no detectable effects on the steady-state levels of other cellular components that regulate endosome-to-TGN transport, including Golgin 97, Golgin 245, or the GARP subunits Vps52 and Vps53 (Fig. S4 B), suggesting that depletion of Cog6 subunit selectively reduces the level of Stx6.

Cog6 interacts directly with the SNARE domain of Stx6 via its N-terminal coiled-coil domain

The profound and unique effect of Cog6 KD on the steady-state level of Stx6 implies that the presence of the Cog6 subunit is crucial for Stx6 stability. This could be explained, at least in part, by a physical interaction between these two proteins. We therefore examined whether Cog6 interacts with Stx6 using

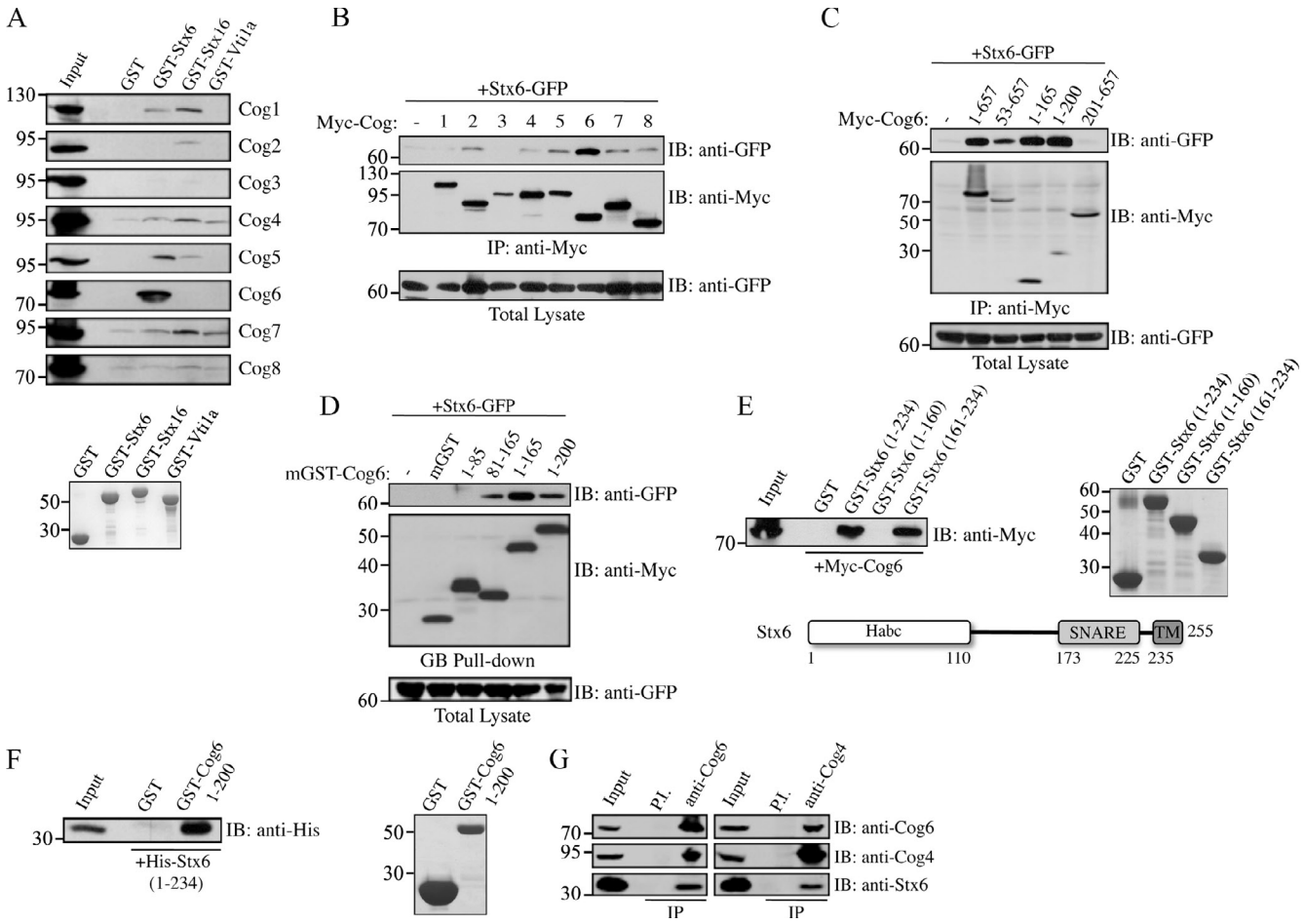

Figure 5. **COG interacts with Stx6 via its Cog6 subunit.** (A) Cog6 interacts with GST-Stx6. The cytosolic portions of Stx6, Stx16, and Vti1a were expressed in bacteria as GST fusion proteins and purified by glutathione-agarose beads (GB). Their ability to interact with the COG subunits was determined by the glutathione-agarose bead pull-down experiment using cell lysates of HEK293 cells expressing each of the eight COG subunits as a Myc-tagged protein. GST bound to glutathione-agarose beads was used as a negative control. The expression levels of the COG subunits are shown in the input control (10%), and those of the GST fusion proteins are shown at the bottom. (B) Cog6 coimmunoprecipitates with Stx6-GFP. The eight Myc-tagged COG subunits were coexpressed with GFP-fused Stx6 in HEK293 cells. Their interaction was determined by immunoprecipitation with the anti-Myc antibody and immunoblotting with the anti-GFP antibody. The expression levels of the COG subunits and Stx6-GFP are shown at the bottom. (C and D) Stx6 interacts with the N-terminal coiled-coil domain of Cog6. The indicated Cog6 truncated mutants were expressed either as Myc-tagged (C) or as GST fusion proteins (D) together with Stx6-GFP in HEK293 cells. Their interaction was determined either by immunoprecipitation with anti-Myc antibody and immunoblotting with anti-GFP antibody (C) or by glutathione-agarose bead pull-down followed by immunoblotting with the anti-GFP antibody (D). The expression levels of Stx6-GFP and Cog6 truncated mutants are shown at the bottom. The numbers indicate the aa residues. (E) Cog6 interacts with the SNARE domain of Stx6. GST fusion proteins expressing the indicated fragments of Stx6 were purified from bacteria, immobilized on glutathione-agarose beads, and incubated with the cell lysate of HEK293 cells expressing a Myc-tagged Cog6. 10% of this lysate (Input) was used for assessing the expression level of Myc-tagged Cog6. GST bound to glutathione-agarose beads was used as a control. The expression level of the different GST fusion proteins was determined by Coomassie blue staining and is shown on the right. The domain organization of Stx6 is shown in the attached scheme. TM, transmembrane. (F) Cog6 interacts directly with Stx6. Cog6 (aa 1–200) was expressed in bacteria as a GST fusion protein, immobilized on glutathione-agarose beads, and incubated with a recombinant His-tagged Stx6 (aa 1–234). The interaction between these recombinant proteins was determined by a glutathione-agarose bead pull-down experiment and, subsequently, by Western blotting using the anti-His antibody. GST was used as a control, and its expression level as well as the expression of GST-Cog6 is shown on the right. (G) Endogenous COG interacts with endogenous Stx6. The HeLa cell lysate was subjected to immunoprecipitation (IP) with either the anti-Cog4 or anti-Cog6 antibody. Preimmune (P.I.) sera were used as controls. The presence of Stx6 in the immunocomplexes of the indicated COG subunits was determined by immunoblotting (IB) with the anti-Stx6 antibody. The interaction between the COG subunits was assessed by immunoblotting with the indicated anti-Cog antibodies. Molecular masses are indicated in kilodaltons.

GST pull-down experiments (Fig. 5 A). GST fusion proteins expressing the cytosolic domains of Stx6, Stx16, or Vti1a were purified from bacteria, immobilized on glutathione-agarose beads, and incubated with lysates of HEK293 cells expressing each of the eight COG subunits. As seen, the Cog6 subunit strongly interacted with Stx6. No detectable interactions between Cog6 and Stx16, Vti1a (Fig. 5 A), VAMP3, VAMP4, or Stx10 (Fig. S5 A) were observed, suggesting that Cog6 selectively interacts with Stx6. To further confirm these observations, we coexpressed GFP-tagged Stx6 and the different COG subunits in HEK293 cells and assessed their interactions by coimmunoprecipitation assay. The results shown in Fig. 5 B clearly demonstrate the strong interaction between Cog6 and Stx6.

To further characterize this interaction, we mapped the binding site of Stx6 in Cog6 using a set of Cog6-truncated mutants. These mutants were prepared according to the predicted secondary structure of Cog6 and were expressed either as Myc-tagged proteins (Fig. 5 C) or GST fusion proteins (Fig. 5 D).

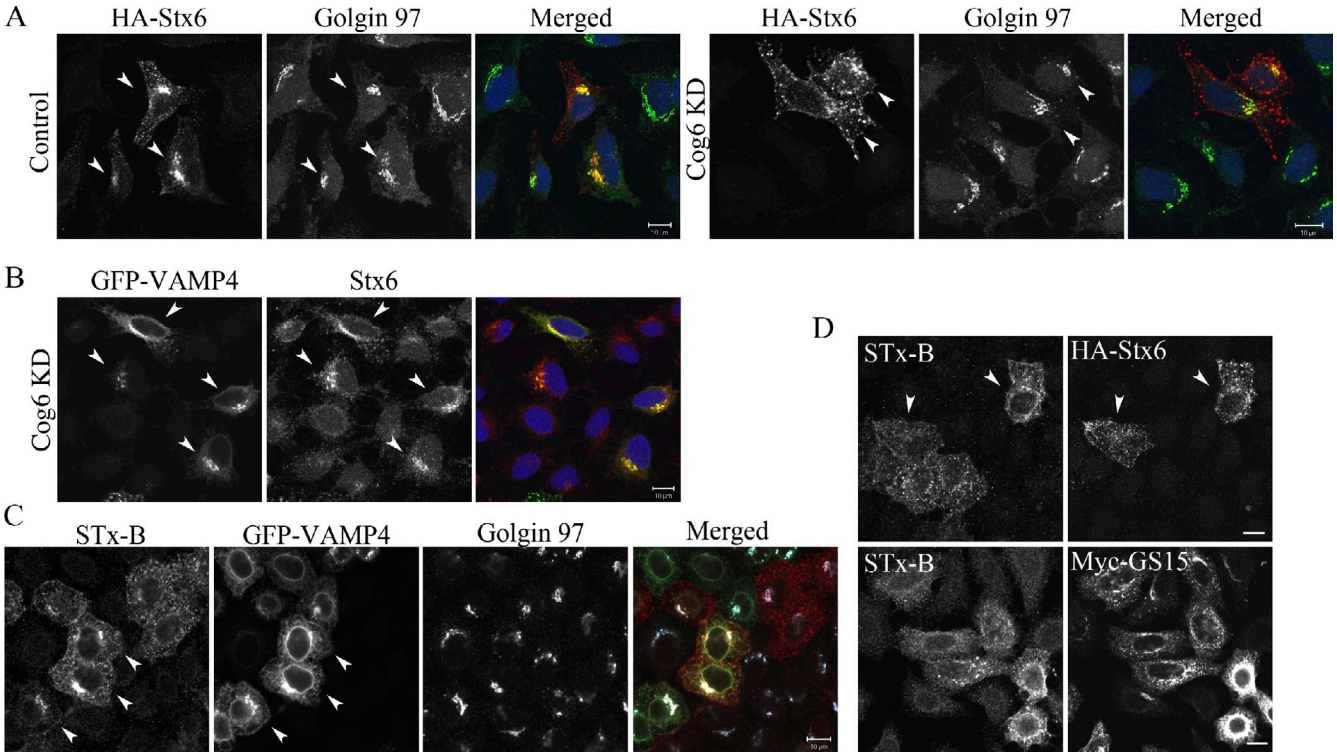

Figure 6. **VAMP4 rescues the TGN localization of Stx6 and endosome-to-TGN trafficking in Cog6-depleted cells.** (A) Exogenous Stx6 failed to localize to the TGN of Cog6-depleted cells. Control (pSUPER-puro) and Cog6-depleted HeLa cells were transiently transfected with an expression vector encoding an HA-tagged Stx6. 24 h later, the cells were fixed and double immunostained with anti-HA and anti–Golgin 97 antibodies. The TGN localization of HA-Stx6 was determined by colocalization with Golgin 97. Arrowheads mark cells expressing HA-Stx6. (B) Overexpression of VAMP4 restored the TGN localization of Stx6 in Cog6-depleted cells. GFP-VAMP4 was overexpressed in Cog6-depleted HeLa cells, and 24 h later, the cells were fixed, immunostained with the anti-Stx6 antibody (red), and analyzed by confocal microscopy. Arrowheads mark the GFP-VAMP4–expressing cells. (C) VAMP4 overexpression restores endosome-to-TGN transport of STx-B in Cog6-depleted cells. Cog6-depleted HeLa cells were transiently transfected with an expression vector encoding GFP-VAMP4. 24 h later, the cells were incubated with recombinant His-tagged STx-B at 4°C for 30 min. The cells were then extensively washed, shifted to 37°C for 45 min, fixed, and double immunostained with anti-His and anti–Golgin 97 antibodies to mark the TGN. As shown, the localization of STx-B in the Golgi of Cog6-depleted cells was detected only in cells that overexpressed VAMP4-GFP, marked by arrowheads. (D) Overexpression of neither Stx6 nor GS15 rescued the endosome-to-TGN transport of STx-B in Cog6-depleted cells. Cog6-depleted HeLa cells were transiently transfected with HA-Stx6 or Myc-tagged GS15 and, 24 h later, incubated with His-tagged STx-B (1 µg/ml) for 30 min at 4°C. Shown are representative confocal images of STx-B localization after a 45-min incubation at 37°C. Cells expressing HA-Stx6 are marked by arrowheads. Bars, 10 µm.

As shown in Fig. 5 C, a mutant containing the first 165 aa of Cog6 interacts strongly with Stx6, similar to the full-length Cog6. Further truncation narrowed down the binding site of Stx6 to aa 81–165 (Fig. 5 D) at the N-terminal amphipathic helical region of Cog6 (Whyte and Munro, 2001, 2002). Collectively, these results suggest that Cog6 binds Stx6 via its N-terminal coiled-coil domain.

Next, we performed the reciprocal experiment and mapped the binding site of Cog6 in Stx6. Several Stx6 truncated mutants were expressed as GST fusion proteins in bacteria, and their interaction with Cog6 was assessed by GST pull-down experiments. As shown in Fig. 5 E, Cog6 interacts with the entire cytoplasmic region of Stx6 (aa 1–234) as well as with its SNARE domain (aa 161–234) but fails to interact with the N-terminal region (aa 1–160) consisting of a trihelical bundle Habc domain and a flexible linker region. These results suggest that Cog6 interacts with the SNARE domain of Stx6 via its N-terminal coiled-coil domain (aa 81–165).

To demonstrate that Cog6 interacts directly with Stx6, we used recombinant proteins expressed in bacteria. The cytoplasmic region of Stx6 (aa 1–234) was expressed as a His-tagged protein, whereas the N-terminal region of Cog6 (aa 1–200) was expressed as a GST fusion protein. The interaction between these recombinant proteins was assessed by a pull-down experiment using GST-Cog6 (aa 1–200) immobilized on glutathione-agarose beads. The results shown in Fig. 5 F strongly suggest that Stx6 interacts directly with Cog6.

We next examined the interaction between endogenous Cog6 and Stx6 by coimmunoprecipitation. As seen in Fig. 5 G, Stx6 was found in Cog6 immunocomplexes as expected but could also be detected in Cog4 immunocomplexes. These results suggest that the entire COG complex interacts with Stx6 via its Cog6 subunit.

Overexpression of VAMP4 restores the Golgi localization of Stx6 and endosome-to-TGN retrograde transport in Cog6-depleted cells

The remarkable effect of Cog6 KD on both the steady-state level and the subcellular distribution of Stx6 (Figs. 3 and 4) implies that the Cog6–Stx6 interaction is involved in both Stx6 stabilization and its TGN localization. However, these two

potential roles could be interdependent. Degradation of Stx6 in the absence of Cog6 would reduce its total steady-state level and, consequently, affect its TGN localization. If this is indeed the case, stabilization of Stx6 should restore the TGN localization of Stx6 in Cog6-depleted cells. To mimic a stabilized Stx6, we ectopically overexpressed it in Cog6-depleted cells and examined its subcellular localization. As shown in Fig. 6 A, HA-tagged Stx6 was mainly localized to the TGN of the control cells, consistent with the localization of the endogenous Stx6 protein (Fig. 3 A). In contrast, it was localized mainly to various punctate cytosolic structures in Cog6-depleted cells and could hardly be detected in the TGN. These results are consistent with the effect of Cog6 KD on the distribution of endogenous Stx6 and its enrichment in the light membrane fraction (Fig. 4 C). Yet, KD of Cog6 also affects the TGN localization of Stx16 and VAMP4 (Fig. 3 B) and also induces their redistribution into the light membrane fraction (Fig. 4 C). These light membranes may represent endosome-derived transport vesicles that fail to tether with the TGN membranes. This possibility is consistent with the role of COG as a tethering factor (Lupashin and Sztul, 2005) and the steady-state distribution of Stx6 and its associated SNAREs (Figs. 3 and 4). Hence, conditions that could overcome the requirement for tethering might restore the recycling of Stx6 and its associated SNAREs and, consequently, their TGN localization in Cog6-depleted cells.

Previous experiments suggest that overexpression of a v-SNARE enhances its interaction with t-SNAREs on the target membranes by mass action, thereby bypassing the requirement for tethering factors (Pfeffer, 1996). Overexpression of the v-SNARE Bet1, for example, suppresses a temperature-sensitive mutation of the tethering factor Uso1p (Sapperstein et al., 1995, 1996). Similarly, high-copy numbers of the v-SNARE Snc2p suppressed the temperature sensitivity of the *sec35-1* strain, which carries a mutation in the Cog2 subunit (VanRheenen et al., 1998). We therefore examined whether overexpression of the v-SNARE VAMP4 could restore the TGN localization of Stx6 in Cog6-depleted cells.

Cog6-depleted cells were transiently transfected with GFP-VAMP4, and the localization of Stx6 was examined by immunofluorescence analysis. As seen in Fig. 6 B, strong immunostaining of Stx6 was observed in the Golgi of Cog6-depleted cells overexpressing the GFP-VAMP4, and colocalization between Stx6 and GFP-VAMP4 was detected. This effect was specific for VAMP4, as neither overexpression of the t-SNAREs Stx16 and Vti1a nor the v-SNARE GS15 could restore the TGN localization of Stx6 in Cog6-depleted cells (Fig. S5 B).

The colocalization between GFP-VAMP4 and Stx6 (Fig. 6 B) suggests that overexpression of VAMP4 restored trans-SNARE complex assembly and, as a consequence, may also restore endosome-to-TGN retrograde trafficking. To explore this possibility, we overexpressed GFP-VAMP4 in Cog6-depleted cells and examined its effect on endosome-to-TGN retrograde transport of STx-B. As shown in Fig. 6 C, overexpression of GFP-VAMP4 rescued the effect of Cog6 KD on STx-B retrograde transport, and 45 min after internalization, STx-B was localized to the Golgi in the majority (~65%; $n = 200$) of Cog6-depleted cells. Overexpression of neither Stx6 nor GS15 (Fig. 6 D) could restore retrograde transport of STx-B in Cog6-depleted cells. Collectively, these results suggest that COG plays two major roles: it is involved in the tethering of endosome-derived vesicles with the TGN membranes, thereby affecting the recycling of SNAREs to the TGN, promoting their assembly, and positively regulates endosome-to-TGN retrograde trafficking. In addition, it stabilizes Stx6 at the TGN via its direct interaction with the Cog6 subunit, thereby stabilizing and/or promoting the assembly of a functional t-SNARE complex on the TGN, which provides a template for v-SNARE binding.

Discussion

In this study, we have identified a novel and direct interaction between the COG complex and the t-SNARE Stx6 and demonstrated that this interaction is mediated by the Cog6 subunit (Fig. 5). In Cog6-depleted HeLa cells, the steady-state level of Stx6 was markedly reduced (Fig. 4 A), the assembly of the Stx6–Stx16–Vti1a–VAMP4 SNARE complex was impaired (Fig. 4 D), and concomitantly, endosome-to-TGN retrograde traffic was substantially inhibited (Figs. 1 and 2). These results suggest that the Cog6–Stx6 interaction stabilizes Stx6, thereby affecting its steady-state level, SNARE complex assembly, and consequently, endosome-to-TGN transport. Consistent with this interpretation, we showed that Stx6 undergoes abnormal proteasomal degradation in Cog6-depleted cells (Fig. 4 E) and that depletion of neither the Cog4 nor Cog8 subunit reduced the steady-state level of Stx6 (Fig. S4 A).

Abnormal proteasomal degradation of the Golgi SNAREs GS28 and GS15 was also observed in cells depleted of different COG subunits (Oka et al., 2004, 2005; Zolov and Lupashin, 2005; Laufman et al., 2009). However, a direct interaction between these SNAREs and the COG has not yet been identified. On the other hand, a direct interaction between certain SM proteins and t-SNAREs was found to stabilize their cognate t-SNAREs through a putative chaperone-like activity of SM proteins. Sly1, for example, interacts directly with the ER t-SNARE Ufe1p, a yeast homologue of Stx18, and protects it from ER-associated degradation (Braun and Jentsch, 2007). Likewise, the SM protein Vps45p interacts with Tlg2p, the yeast homologue of Stx16, and protects it from proteasomal degradation (Bryant and James, 2001). Hence, it could be that Cog6 also induces conformational changes of its associated t-SNARE Stx6, thereby regulating its stability.

Nevertheless, SM proteins generally interact with the N-terminal regions of syntaxins (Südhof and Rothman, 2009), whereas Cog6 interacts with the SNARE domain of Stx6 (Fig. 5 E) via its N-terminal coiled-coil domain (aa 81–165) (Fig. 5 D). Interestingly, the N-terminal coiled-coil domain of Cog4 also interacts with the SNARE domain of Stx5 (Shestakova et al., 2007), whereas the N-terminal coiled-coil domains of the Vps53 and Vps54 subunits of the mammalian GARP complex interact with the SNARE motifs of Stx6, Stx16, and VAMP4 (Pérez-Victoria and Bonifacino, 2009). These N-terminal coiled-coil domains of GARP and COG subunits share sequence similarity with components of the exocyst complex (Whyte and

Munro, 2001, 2002) and may also share a common SNARE domain-binding capability.

Depletion of GARP subunits by RNAi impaired the retrieval of TGN46 as well as CI-MPR to the TGN and caused a redistribution of Stx16, VAMP4, and Vti1a from the TGN (Pérez-Victoria and Bonifacino, 2009; Pérez-Victoria et al., 2010). Similarly, KD of Cog6 had a profound effect on the steady-state distribution of these SNAREs (Figs. 2, 3, and 4 C) but also markedly affected their steady-state levels (Fig. 4, A and C). The effect of COG on the steady-state levels of these SNAREs seems to be unique, as it was not observed in response to KD of either GARP or GCC88 (Lieu et al., 2007; Pérez-Victoria and Bonifacino, 2009).

GCC88 does not interact with Stx6, but its depletion dramatically perturbs the TGN localization of Stx6 without affecting either its steady-state level or the steady-state distribution of its associated SNAREs. Interestingly, overexpression of Stx6 in GCC88-depleted cells rescued the recycling of TGN38 (Lieu et al., 2007). The ability of exogenous Stx6 to rescue the transport defect of GCC88-depleted cells might be attributed to its proper TGN localization. Consistent with this possibility, exogenous Stx6 overexpressed in Cog6-depleted cells failed to localize to the TGN (Fig. 6 A) and, concomitantly, could not restore the endosome-to-TGN transport defects (Fig. 6 D). On the other hand, overexpression of VAMP4 restored the TGN localization of Stx6 as well as endosome-to-TGN trafficking (Fig. 6, B and C). These results demonstrate a direct link between the TGN localization of Stx6 and endosome-to-TGN transport.

Yet, it is unclear why exogenous Stx6 failed to localize to the TGN of Cog6-depleted cells (Fig. 6 A). One potential explanation is that the direct interaction with Cog6 stabilizes its interactions with the other t-SNAREs on the TGN, thereby influencing its TGN localization. The interaction of Stx6 with the other t-SNAREs, especially with Stx16, appears to influence its TGN localization. A previous study has shown that depletion of Stx16 affects the TGN localization of Stx6 (Wang et al., 2005) and that exogenous Stx6 is properly localized to the TGN of GCC88-depleted cells. In these cells, the TGN localization of endogenous Stx16, Vti1a, or VAMP3/4 was unaffected (Lieu et al., 2007). In contrast, the TGN localization of Stx16 was markedly reduced in Cog6-depleted cells (Fig. 3 B), and concomitantly, exogenous Stx6 failed to localize to the TGN. This simple explanation may only partially explain the influence of Cog6 depletion on Stx6. Hence, we propose that COG plays two major roles that enhance each other. It affects the steady-state level of Stx6 through a direct interaction with Cog6. This interaction might induce conformational changes or perhaps enables posttranslational modifications in the Stx6 protein. These modifications could stabilize Stx6 and/or its interactions with the other t-SNAREs on the TGN, thereby contributing to t-SNARE complex assembly. On the other hand, COG affects the recycling of the t-SNAREs to the TGN by its tethering activity. Thus, in the absence of Cog6, the recycling of the t-SNAREs to the TGN is impaired, and concomitantly, the ability of Stx6 to interact with the other t-SNAREs is affected. Therefore, Stx6 remains in an unbound form and is subjected to rapid degradation. This could explain why the steady-state level of Stx6 is selectively reduced in Cog6-depleted cells despite the fact that all the other SNAREs are also enriched in intermediate transport elements (Fig. 4 C). Consistent with this dual role, we showed that overexpression of VAMP4 could bypass the requirement for COG (Fig. 6, B and C), suggesting that COG indeed functions as a tethering factor.

Previous experiments suggest that both tethering factors and SNAREs can contribute to vesicle docking and that overexpression of SNAREs can compensate for tethering defects (Wiederkehr et al., 2004). Perhaps the most relevant example is related to the *sec35* mutation, which can be bypassed by overexpression of the v-SNARE protein Snc2p (VanRheenen et al., 1998). Snc2p is very similar to Snc1p (Protopopov et al., 1993), the yeast homologue of VAMP3, and is functionally related to VAMP4 (Paumet et al., 2001). These genetic studies in yeast and the observations described in this study strongly suggest that COG is involved in the tethering of endosome-derived vesicles to the TGN membranes. Overexpression of VAMP4 could bypass the requirement for COG because of the presence of multiple, locally concentrated v-SNARE proteins. These locally concentrated v-SNAREs could interact directly with the residual t-SNAREs (Stx16, Stx6, and Vti1a) on the TGN and, consequently, enable the fusion of endosome-derived vesicles. Over time, the fusion of these vesicles would restore the TGN localization of the t-SNAREs and, consequently, rescue the transport defects. Collectively, our findings strongly suggest that COG is involved in both the stabilization of the t-SNARE complex at the TGN and in the tethering of endosome-derived vesicles with the TGN membranes, thereby affecting endosome-to-TGN retrograde trafficking.

The capability of a given tethering factor, the COG, to regulate both intra-Golgi and endosome-to-TGN retrograde transport, could provide a mechanism for coordination between the two trafficking pathways. These two transport routes must be tightly coordinated to maintain the structural and functional integrity of the Golgi complex. Although the Stx5–GS28–Ykt6–GS15 SNARE complex has been implicated in the regulation of both intra-Golgi and endosome to Golgi retrograde transport, we show here that overexpression of VAMP4, but not of GS15, could restore the endosome-to-TGN transport defect of STx-B in Cog6-depleted cells (Fig. 6, C and D). These results strongly suggest that the Stx6–Stx16–Vti1a–VAMP4 complex cooperates with COG in endosome-to-TGN trafficking, whereas the Stx5–GS28–Ykt6–GS15 SNARE complex cooperates with COG in intra-Golgi retrograde transport. This capability of COG is mediated, at least in part, by direct interaction of COG subunits with different components of the fusion machinery: Cog4 interacts directly with Stx5 and Sly1 (Shestakova et al., 2007; Laufman et al., 2009), whereas Cog6 interacts directly with Stx6. Whether other COG subunits interact directly with other components of the fusion machinery of these trafficking pathways is yet to be determined.

An important question emerging from our experiments is related to the multiple tethering factors that regulate endosome-to-TGN transport and, in some cases, even use the same fusion machinery. It could be that multiple tethering factors are

required for efficient recycling of SNAREs that regulate this transport route. Components of the Stx6–Stx16–Vti1a–VAMP4 SNARE complex are involved in different transport steps and are assembled into different SNARE complexes. VAMP4, for example, is a multifunctional v-SNARE that is required in the endocytic pathway as well as for the fusion of secretory vesicles with the plasma membrane (McNew et al., 2000; Hong, 2005). Similarly, Stx6 appears to take part in a variety of membrane fusion events as part of different SNARE complexes (Wendler and Tooze, 2001). Hence, multiple tethering factors could provide overlapping backup mechanisms that ensure efficient recycling of these SNAREs, thereby contributing to the coordination of distinct fusion events. Consistent with this role, KD of either GARP, GCC88, GCC185, or COG, as shown here, attenuates rather than abolishes endosome-to-TGN transport of certain cargoes. Yet, it could be that different tethering factors are responsible for the transport of different cargoes using the same SNARE complex. Identification of additional cargo molecules that use this trafficking route and elucidating the mechanisms by which different tethering factors regulate their transport would greatly contribute to the current understanding of fusion events at the TGN.

Materials and methods

Antibodies, reagents, and chemicals

Polyclonal antibodies against Cog3, Cog4, Cog7, and Golgin 97 as well as the monoclonal antibody against GS28 were previously described (Subramaniam et al., 1995; Lu et al., 2004; Laufman et al., 2009). Polyclonal antibodies against Cog2 (aa 500–578), Cog6 (aa 103–230), and Stx6 (aa 1–235) were raised in rabbits immunized with recombinant GST fusion proteins consisting of the indicated aa residues. Polyclonal antibodies against Cog5 and Cog8 were provided by D. Ungar (York University, York, England, UK), and a polyclonal antibody against Cog1 was provided by M. Krieger (Massachusetts Institute of Technology, Cambridge, MA). Polyclonal antibodies against Stx16 and Stx5 were a gift from B.L. Tang (National University of Singapore, Singapore) and from Z. Elazar (Weizmann Institute of Science, Rehovot, Israel), respectively. Polyclonal anti-VAMP4 and anti-Vti1a antibodies were purchased from Synaptic Systems and from Proteintech Group, Inc., respectively. Monoclonal anti-GS15, anti-Stx6, anti-EEA1, and anti–γ-adaptin antibodies were purchased from BD. Monoclonal anti–CI-MPR and anti-His antibodies and polyclonal anti-EEA1 and anti–CI-MPR antibodies were purchased from Abcam. The sheep anti-TGN46 antibody was purchased from AbD Serotec. The monoclonal anti–KDEL receptor (KDELR) antibody was obtained from Santa Cruz Biotechnology, Inc., and the polyclonal anti–mannosidase II antibody was obtained from the University of Georgia. Polyclonal antibodies against Vps52 and Vps53 and the polyclonal anti-Arf1 antibody were provided by J. Bonifacino (National Institutes of Health, Bethesda, MD) and by B. Aroeti (Hebrew University, Jerusalem, Israel), respectively. The mouse anti–α-tubulin antibody was purchased from Sigma-Aldrich. Alexa Fluor 488 donkey anti–mouse and anti–rabbit IgGs were purchased from Invitrogen. Cy3 (cyanine 3)-conjugated goat anti–rabbit and goat anti–mouse IgGs as well as the Cy5-conjugated goat anti–rabbit IgG were purchased from Jackson ImmunoResearch Laboratories, Inc.

Protein A–agarose beads were purchased from Repligen Corp. Ni-nitrilotriacetic acid agarose beads were obtained from QIAGEN, whereas the anti–mouse IgG conjugated to agarose beads, Hoechst 33342, MG132, and chloroquine was purchased from Sigma-Aldrich.

DNA constructs

The DNA constructs encoding the different Myc-tagged COG subunits have been described previously (Loh and Hong, 2002, 2004). Truncated Cog6 mutants were produced by subcloning of the corresponding PCR products into either the pCMV-neomycin-Myc and the mammalian GST expression vectors or the pGEX-4T-1 bacterial expression vector, as indicated in the legend of Fig. 5. The following sense and antisense primers have been used for PCR amplifications: Cog6 (aa 53–657), 5′-AACGCACTCGAGATGTTAGAAGCTCTCAAGGC-3′ and 5′-AATGGTACCTCAGGAAAGAAGCGTCTGCAC-3′; Cog6 (aa 1–165), 5′-AAAGGATCCATGGCAGAGGGCAGCGGG-3′ and 5′-AAACTCGAGTCAAGAAGTCAGTTGGAACTTGG-3′; Cog6 (aa 1–200), 5′-AAACTCGAGATGGCAGAGGGCAGCGGG-3′ and 5′-CACGGTACCCTAACGCAAGAGAACTTTGAC-3′; Cog6 (aa 201–657), 5′-AAACTCGAGCGTACAAATCAACAAACGGC-3′ and 5′-AATGGTACCTCAGGAAAGAAGCGTCTGCAC-3′; Cog6 (aa 1–85), 5′-AAAGGATCCATGGCAGAGGGCAGCGGG-3′ and 5′-AAAGGTACCTCAGGCTAAACTTTTACGTTCAATATCTCCACG-3′; and Cog6 (aa 81–165), 5′-AAAGGATCCCGTAAAAGTTTAGCCATCAATGAAG-3′ and 5′-AAACTCGAGTCAAGAAGTCAGTTGGAACTTGG-3′.

The mammalian expression vector encoding the GFP-Stx6 was provided by J.E. Pessin (Stony Brook University, New York, NY). Mammalian expression vectors encoding the cytosolic fragments of the human Stx6, Stx16, and Vti1a were provided by S.R. Pfeffer (Stanford University School of Medicine, Stanford, CA). These fragments were subcloned into the pGEX-4T-1 bacterial expression vector. The truncated Stx6 mutants were produced by subcloning of the corresponding PCR products into either pGEX-4T-1 or pCDFDuet-1 bacterial expression vectors. The following sense and antisense primers have been used for PCR amplifications: Stx6 (aa 1–160), 5′-AGAGGATCCTCCATGGAGGACCCCTTCTTTG-3′ and 5′-AAACTCGAGCTACTGTGCCTGCTGCTCCTCAATG-3′; and Stx6 (aa 161–234), 5′-AACGGATCCCAGCAGCAGTTGATCGTGGAAC-3′ and 5′-AAACTCGAGCTATTGGCGCCGATCACTGGTC-3′.

The mammalian expression vector encoding GFP-VAMP4 has been previously described (Zeng et al., 2003). Truncated VAMP4 lacking its transmembrane domain was produced by PCR and subcloned into pGEX-4T-1. The following primers were used for PCR amplification: 5′-AACGGATCCATGCCTCCCAAGTTCAAG-3′and5′-AGACTCGAGTCAGGCTTTTATTTTGCATCCAC-3′. Mammalian expression vectors encoding HA-Stx16 and HA-Vti1a were provided by G.F.V. Mollard (Bielefeld University, Bielefeld, Germany).

The cDNA of GS15 was PCR amplified from a mouse spleen cDNA library, sequenced, and subcloned into pCMV-neomycin-Myc mammalian expression vector. The following sense and antisense oligonucleotide primers were used: 5′-AAAGGATCCTATGGCGGACTGGGCTCGG-3′ and 5′-AAACTCGAGTCACGTCCTTGCCCTGGAC-3′.

shRNA constructs. The mammalian pSUPER-puro vector was used for expression of shRNAs corresponding to nucleotides 1,242–1,260 (5′-GGAGCTAATTGGCTTATAT-3′) of the human Cog4 cDNA and nucleotides 1,512–1,531 (5′-GACCTTGTTCCGTATTTAA-3′) of the human Cog8 cDNA. Two shRNAs have been used to knock down the expression of Cog6 shRNA1 and shRNA2 corresponding to nucleotides 1,591–1,609 (5′-GCACATTTGGACACACTTA-3′) and 348–366 (5′-AGATATGACAAGTCGCCTA-3′) of the human Cog6 cDNA, respectively. shRNA1 has been chosen for further analysis shown in the figures in this paper.

Cell culture, transfection, and immunofluorescence microscopy

HEK293 and HeLa cells were grown in DME supplemented with 10% fetal bovine serum, 100 µg/ml penicillin, and 100 µg/ml streptomycin. The cells were transfected using either the calcium-phosphate method or transfection reagent (FuGENE HD; Roche). Stable HeLa cell lines depleted of the Cog6 subunit were established using the pSUPER-puro vector encoding shRNA1 (nucleotides 1,591–1,609) as previously described for Cog4 (Laufman et al., 2009). A stable HeLa cell line harboring an empty pSUPER-puro vector was established and used as a control. These stable HeLa cell lines were used in all the transport assays and rescue experiments described in this paper (Figs. 1 and 6). Transient transfections with the Cog6 shRNA1 construct or the pSUPER-puro empty vector were performed for all the localization experiments and the biochemical analysis. In brief, HeLa cells grown on coverslips or in 90-mm tissue culture dishes were transiently transfected with the Cog6 shRNA1 construct or pSUPER-puro vector using FuGENE HD. 24 h after transfection, the cells were either incubated with regular medium for 72 h and then analyzed by immunofluorescence or were incubated with 1 µg/ml puromycin for 72 h and then analyzed by the indicated biochemical assay as described in the legends of Figs. 4, S1, and S4.

For immunofluorescence analysis, control and Cog6-depleted HeLa cells were grown on coverslips, washed with PBS, and fixed in 1% paraformaldehyde in either PBS or KM buffer (10 mM 2-(*N*-morpholino)ethanesulfonic acid, pH 6.2, 10 mM NaCl, 1.5 mM $MgCl_2$, and 2.5% glycerol) for 20 min at room temperature. Fixed cells were then permeabilized with either 0.1% Triton X-100 or 0.03% saponin (VAMP4 staining) in PBS and immunostained at room temperature essentially as previously described

(Litvak et al., 2002). In brief, the fixed cells were incubated for 30 min in blocking buffer (10 mM Tris, pH 7.5, 150 mM NaCl, 2% BSA, 1% glycine, 10% goat serum, and 0.1% Triton X-100 or 0.03% saponin) and then for 1 h with the indicated primary antibodies diluted in the blocking buffer as described in Figs. 1, 2, 3, and 6 and in their legends. The cells were then washed with PBS and incubated with the appropriate fluorescence-labeled secondary antibodies for 1 h. After washing in PBS, the cells were incubated for 5 min with 2 ng/µl Hoechst 33342, washed again with PBS, and mounted on microscopic slides using mounting media (10 mM phosphate buffer, pH 8.0, 16.6% wt/vol Mowiol 4-88, and 33% glycerol).

The specimens were analyzed by a confocal laser-scanning microscope (LSM 510; Carl Zeiss) equipped with a 63×/1.4 oil differential interference contrast M27 objective lens (Plan Apochromat; Carl Zeiss) using the 488-, 543-, and either 405- or 633-nm excitation for fluorescein, Cy3 epifluorescence, and either 4,6-diamidino-2-phenylindole (Hoechst) or Cy5, respectively. Images were acquired using the LSM 510 software.

Cell extracts, subcellular fractionation, immunoprecipitations, and pull-down experiments

Cell extracts were prepared by solubilizing HEK293 or HeLa cells, as indicated in the legends of Figs. 4, 5, S1, S4, and S5, in lysis buffer (1% Triton X-100, 20 mM Hepes, pH 7.5, 100 mM NaCl, 5 mM $MgCl_2$, 1 mM PMSF, 10 µg/ml leupeptin, and 10 µg/ml aprotinin) for 1 h on ice. Cell lysates were centrifuged at 15,000 *g* for 15 min at 4°C. Protein concentration of the supernatants was determined by Bradford assay (Bio-Rad Laboratories), and equal protein amounts were analyzed by SDS-PAGE and Western blotting using antibodies against the indicated SNAREs or the COG subunits to determine their steady-state levels as described in Figs. 4 (A and B), S1 B, and S4 A. Immunoprecipitations were performed essentially as described previously (Amarilio et al., 2005). In brief, cell lysates were incubated for 3 h at 4°C with either agarose–protein A (Repligen Corp.) or agarose anti–mouse IgG beads bound to the indicated polyclonal or mouse monoclonal antibodies, respectively. The beads were washed three times with lysis buffer, boiled in SDS sample buffer, and separated by SDS-PAGE. Immunoprecipitation of SNARE complexes was performed after treatment with NEM as previously described (Pérez-Victoria and Bonifacino, 2009). In brief, control or Cog6-depleted HeLa cells were incubated in medium containing 1 mM NEM for 15 min on ice, washed with PBS, and then incubated in medium containing 2 mM DTT for 15 min on ice. The cells were then incubated in complete medium for 30 min at 37°C, solubilized on ice in lysis buffer, and subjected to immunoprecipitation for 3 h at 4°C with agarose–protein A beads bound to a rabbit anti-Vti1a antibody. The beads were washed three times with lysis buffer, boiled in SDS sample buffer, and separated by SDS-PAGE.

Pull-down experiments were performed as described previously (Laufman et al., 2009). In brief, GST and GST fusion proteins were expressed in bacteria and purified by standard procedures (GE Healthcare) using glutathione-agarose beads. The beads were then incubated with cell lysates of HEK293 cells expressing the indicated proteins for 2 h at 4°C. The samples were washed twice in buffer containing 20 mM Hepes, pH 7.5, 250 mM NaCl, and 1 mM DTT followed by three washes in buffer containing 20 mM Hepes, pH 7.5, 250 mM NaCl, 1% Triton X-100, and 1 mM DTT and, finally, with buffer containing 20 mM Hepes, pH 7.5, 100 mM NaCl, and 1 mM DTT. The bound proteins were analyzed by Western blotting. For direct binding assays, His-tagged Stx6 (aa 1–234) was purified from bacteria on a nickel column according to the manufacturer's instructions (QIAGEN), incubated with either GST or GST-Cog6 (aa 1–200) bound to glutathione-agarose beads, washed as described in this paragraph, and analyzed by Western blotting.

For subcellular fractionation, cells were resuspended in 20 mM Hepes, pH 7.4, supplemented with protease inhibitors, and incubated on ice for 30 min. Cells were disrupted by 20 passages through a 23-gauge needle. Subcellular fractions were obtained using differential centrifugation at 4°C. The postnuclear supernatant was obtained by centrifugation at 1,000 *g* for 5 min. Heavy membranes containing ER and Golgi membranes were pelleted at 10,000 *g* for 10 min. Light membranes containing various transport vesicles were pelleted at 100,000 *g* for 1 h. All membrane pellets were resuspended in volumes equal to the volume of the original lysate. Densitometric analysis was performed using the ImageJ software (National Institutes of Health).

Transport assays

Retrograde transport from the Golgi complex. Retrograde transport of mannosidase II and KDELR from the Golgi complex was assessed by brefeldin A (BFA) treatment and by a temperature block (15°C), respectively, as we previously described (Laufman et al., 2009). In brief, control and Cog6-depleted HeLa stable cell lines were either treated with 5 µg/ml BFA or incubated at 15°C for the indicated time points. The cells were then fixed, immunostained with anti–mannosidase II or anti-KDELR antibodies, respectively, and analyzed by confocal microscopy.

Shiga toxin transport assay. The bacterial expression vector pCRT7 (Invitrogen) encoding the His-tagged STx-B was a gift from D.B. Haslam (Washington University School of Medicine, St. Louis, MO). Recombinant STx-B was isolated from periplasmic extracts of *Escherichia coli* BL21 (pLysS) cells (Invitrogen). The cells were grown at 37°C in Luria-Bertani broth to an optical density of 0.6 at 600 nm and then were grown for an additional 2 h in the presence of 1 mM isopropylthiogalactoside. Periplasmic extraction was performed by osmotic shock, and the recombinant protein was purified on a nickel column according to the manufacturer's instructions (QIAGEN). Control and Cog6-depleted HeLa stable cell lines were incubated in DME containing 20 mM Hepes, pH 7.4, and 1 µg/ml purified recombinant STx-B protein for 30 min at 4°C. The cells were then washed with PBS and incubated in a complete growth media at 37°C for the indicated time periods as described in Fig. 1 A. Cells were then fixed, double immunostained with anti-His and anti–Golgin 97 antibodies or with anti-His and anti-EEA1 antibodies, and analyzed by confocal microscopy.

Antibody uptake assay. Control and Cog6-depleted HeLa stable cell lines were transfected with a mammalian expression vector encoding HA-TGN38. 48 h later, the cells were incubated at 37°C in medium containing 1.5 µg/ml anti-HA monoclonal antibody for the different time periods (3, 15, and 30 min and 1 and 2 h). The cells were then extensively washed with PBS, fixed, and stained with rabbit anti–Golgin 97 antibodies followed by staining with Cy3 anti–mouse and Alexa Fluor anti–rabbit secondary antibodies.

Quantitative analysis of transport assays. Confocal images of arbitrary fields from two independent experiments were acquired for both control and Cog6-depleted HeLa cells (n = 200–300, as indicated in the Results and in the legend of Fig. S2) using the LSM 510 software. The images were scored visually, and colocalization between the TGN marker Golgin 97 (Fig. 1 A, green) and either STx-B (Fig. 1 A, red) or TGN38 (Fig. 1 A, red) in the Golgi region was displayed as yellow in the merged image. Cells with a yellow signal in the Golgi were counted as positive. The percentage of cells exhibiting TGN-localized TGN38 or STx-B is shown in Fig. S2 B or described in the results of Fig. 1 A, respectively. For precise quantitation of TGN localization, the colocalization between Golgin 97 and either STx-B or TGN38 was measured using the colocalization function of the LSM 510 software. Colocalization was determined by measuring the ratio between Golgi-associated STx-B or Golgi-associated TGN38 fluorescence (marked by Golgin 97) to their total fluorescence in the cell. The data shown are mean values ± SD (n = 30).

Online supplemental material

Fig. S1 shows that depletion of the Cog6 subunit by shRNA affects the steady-state levels and the Golgi localization of COG subunits and attenuates retrograde transport from the Golgi complex. Fig. S2 shows that depletion of the Cog6 subunit affects retrograde transport of STx-B and TGN38 to the TGN. Fig. S3 shows that depletion of Cog6 has no effect on the Golgi localization of Stx5 and GS28. Fig. S4 shows that depletion of either Cog4 or Cog8 subunits has no marked effect on the steady-state level of Stx6 and that depletion of the Cog6 subunit has no effect on the steady-state levels of cellular regulators of endosome-to-TGN trafficking. Fig. S5 shows that Cog6 does not interact with VAMP3, VAMP4, or Stx10 and that overexpression of Stx16, Vti1a, or GS15 failed to restore the TGN localization of Stx6 in Cog6-depleted cells. Online supplemental material is available at http://www.jcb.org/cgi/content/full/jcb.201102045/DC1.

Sima Lev is the incumbent of the Joyce and Ben B. Eisenberg Chair of Molecular Biology and Cancer Research. This work was supported by the Minerva foundation with funding from the Federal German Ministry for Education and Research.

Submitted: 8 February 2011
Accepted: 5 July 2011

References

Amarilio, R., S. Ramachandran, H. Sabanay, and S. Lev. 2005. Differential regulation of endoplasmic reticulum structure through VAP-Nir protein interaction. *J. Biol. Chem.* 280:5934–5944. doi:10.1074/jbc.M409566200

Amessou, M., A. Fradagrada, T. Falguières, J.M. Lord, D.C. Smith, L.M. Roberts, C. Lamaze, and L. Johannes. 2007. Syntaxin 16 and syntaxin 5 are required for efficient retrograde transport of several exogenous and endogenous cargo proteins. *J. Cell Sci.* 120:1457–1468. doi:10.1242/jcs.03436

Bock, J.B., J. Klumperman, S. Davanger, and R.H. Scheller. 1997. Syntaxin 6 functions in trans-Golgi network vesicle trafficking. *Mol. Biol. Cell*. 8:1261–1271.

Bonifacino, J.S., and R. Rojas. 2006. Retrograde transport from endosomes to the trans-Golgi network. *Nat. Rev. Mol. Cell Biol.* 7:568–579. doi:10.1038/nrm1985

Braun, S., and S. Jentsch. 2007. SM-protein-controlled ER-associated degradation discriminates between different SNAREs. *EMBO Rep.* 8:1176–1182. doi:10.1038/sj.embor.7401105

Bruinsma, P., R.G. Spelbrink, and S.F. Nothwehr. 2004. Retrograde transport of the mannosyltransferase Och1p to the early Golgi requires a component of the COG transport complex. *J. Biol. Chem.* 279:39814–39823. doi:10.1074/jbc.M405500200

Bryant, N.J., and D.E. James. 2001. Vps45p stabilizes the syntaxin homologue Tlg2p and positively regulates SNARE complex formation. *EMBO J.* 20:3380–3388. doi:10.1093/emboj/20.13.3380

Chatterton, J.E., D. Hirsch, J.J. Schwartz, P.E. Bickel, R.D. Rosenberg, H.F. Lodish, and M. Krieger. 1999. Expression cloning of LDLB, a gene essential for normal Golgi function and assembly of the ldlCp complex. *Proc. Natl. Acad. Sci. USA*. 96:915–920. doi:10.1073/pnas.96.3.915

Foulquier, F., E. Vasile, E. Schollen, N. Callewaert, T. Raemaekers, D. Quelhas, J. Jaeken, P. Mills, B. Winchester, M. Krieger, et al. 2006. Conserved oligomeric Golgi complex subunit 1 deficiency reveals a previously uncharacterized congenital disorder of glycosylation type II. *Proc. Natl. Acad. Sci. USA*. 103:3764–3769. doi:10.1073/pnas.0507685103

Foulquier, F., D. Ungar, E. Reynders, R. Zeevaert, P. Mills, M.T. García-Silva, P. Briones, B. Winchester, W. Morelle, M. Krieger, et al. 2007. A new inborn error of glycosylation due to a Cog8 deficiency reveals a critical role for the Cog1-Cog8 interaction in COG complex formation. *Hum. Mol. Genet.* 16:717–730. doi:10.1093/hmg/ddl476

Ganley, I.G., E. Espinosa, and S.R. Pfeffer. 2008. A syntaxin 10–SNARE complex distinguishes two distinct transport routes from endosomes to the trans-Golgi in human cells. *J. Cell Biol.* 180:159–172. doi:10.1083/jcb.200707136

Ghosh, P., N.M. Dahms, and S. Kornfeld. 2003. Mannose 6-phosphate receptors: new twists in the tale. *Nat. Rev. Mol. Cell Biol.* 4:202–212. doi:10.1038/nrm1050

Ghosh, R.N., W.G. Mallet, T.T. Soe, T.E. McGraw, and F.R. Maxfield. 1998. An endocytosed TGN38 chimeric protein is delivered to the TGN after trafficking through the endocytic recycling compartment in CHO cells. *J. Cell Biol.* 142:923–936. doi:10.1083/jcb.142.4.923

Hong, W. 2005. SNAREs and traffic. *Biochim. Biophys. Acta*. 1744:120–144. doi:10.1016/j.bbamcr.2005.03.014

Johannes, L., and V. Popoff. 2008. Tracing the retrograde route in protein trafficking. *Cell*. 135:1175–1187. doi:10.1016/j.cell.2008.12.009

Klumperman, J., R. Kuliawat, J.M. Griffith, H.J. Geuze, and P. Arvan. 1998. Mannose 6–phosphate receptors are sorted from immature secretory granules via adaptor protein AP-1, clathrin, and syntaxin 6–positive vesicles. *J. Cell Biol.* 141:359–371. doi:10.1083/jcb.141.2.359

Kranz, C., B.G. Ng, L. Sun, V. Sharma, E.A. Eklund, Y. Miura, D. Ungar, V. Lupashin, R.D. Winkel, J.F. Cipollo, et al. 2007. COG8 deficiency causes new congenital disorder of glycosylation type IIh. *Hum. Mol. Genet.* 16:731–741. doi:10.1093/hmg/ddm028

Laufman, O., A. Kedan, W. Hong, and S. Lev. 2009. Direct interaction between the COG complex and the SM protein, Sly1, is required for Golgi SNARE pairing. *EMBO J.* 28:2006–2017. doi:10.1038/emboj.2009.168

Lieu, Z.Z., M.C. Derby, R.D. Teasdale, C. Hart, P. Gunn, and P.A. Gleeson. 2007. The golgin GCC88 is required for efficient retrograde transport of cargo from the early endosomes to the trans-Golgi network. *Mol. Biol. Cell*. 18:4979–4991. doi:10.1091/mbc.E07-06-0622

Litvak, V., D. Tian, S. Carmon, and S. Lev. 2002. Nir2, a human homolog of *Drosophila melanogaster* retinal degeneration B protein, is essential for cytokinesis. *Mol. Cell. Biol.* 22:5064–5075. doi:10.1128/MCB.22.14.5064-5075.2002

Loh, E., and W. Hong. 2002. Sec34 is implicated in traffic from the endoplasmic reticulum to the Golgi and exists in a complex with GTC-90 and ldlBp. *J. Biol. Chem.* 277:21955–21961. doi:10.1074/jbc.M202326200

Loh, E., and W. Hong. 2004. The binary interacting network of the conserved oligomeric Golgi tethering complex. *J. Biol. Chem.* 279:24640–24648. doi:10.1074/jbc.M400662200

Lu, L., G. Tai, and W. Hong. 2004. Autoantigen Golgin-97, an effector of Arl1 GTPase, participates in traffic from the endosome to the trans-golgi network. *Mol. Biol. Cell*. 15:4426–4443. doi:10.1091/mbc.E03-12-0872

Luke, M.R., L. Kjer-Nielsen, D.L. Brown, J.L. Stow, and P.A. Gleeson. 2003. GRIP domain-mediated targeting of two new coiled-coil proteins, GCC88 and GCC185, to subcompartments of the trans-Golgi network. *J. Biol. Chem.* 278:4216–4226. doi:10.1074/jbc.M210387200

Lupashin, V., and E. Sztul. 2005. Golgi tethering factors. *Biochim. Biophys. Acta*. 1744:325–339. doi:10.1016/j.bbamcr.2005.03.013

Mallard, F., C. Antony, D. Tenza, J. Salamero, B. Goud, and L. Johannes. 1998. Direct pathway from early/recycling endosomes to the Golgi apparatus revealed through the study of shiga toxin B-fragment transport. *J. Cell Biol.* 143:973–990. doi:10.1083/jcb.143.4.973

Mallard, F., B.L. Tang, T. Galli, D. Tenza, A. Saint-Pol, X. Yue, C. Antony, W. Hong, B. Goud, and L. Johannes. 2002. Early/recycling endosomes-to-TGN transport involves two SNARE complexes and a Rab6 isoform. *J. Cell Biol.* 156:653–664. doi:10.1083/jcb.200110081

McNew, J.A., F. Parlati, R. Fukuda, R.J. Johnston, K. Paz, F. Paumet, T.H. Söllner, and J.E. Rothman. 2000. Compartmental specificity of cellular membrane fusion encoded in SNARE proteins. *Nature*. 407:153–159. doi:10.1038/35025000

Meyer, C., D. Zizioli, S. Lausmann, E.L. Eskelinen, J. Hamann, P. Saftig, K. von Figura, and P. Schu. 2000. mu1A-adaptin-deficient mice: lethality, loss of AP-1 binding and rerouting of mannose 6-phosphate receptors. *EMBO J.* 19:2193–2203. doi:10.1093/emboj/19.10.2193

Oka, T., D. Ungar, F.M. Hughson, and M. Krieger. 2004. The COG and COPI complexes interact to control the abundance of GEARs, a subset of Golgi integral membrane proteins. *Mol. Biol. Cell*. 15:2423–2435. doi:10.1091/mbc.E03-09-0699

Oka, T., E. Vasile, M. Penman, C.D. Novina, D.M. Dykxhoorn, D. Ungar, F.M. Hughson, and M. Krieger. 2005. Genetic analysis of the subunit organization and function of the conserved oligomeric golgi (COG) complex: studies of COG5- and COG7-deficient mammalian cells. *J. Biol. Chem.* 280:32736–32745. doi:10.1074/jbc.M505558200

Paumet, F., B. Brügger, F. Parlati, J.A. McNew, T.H. Söllner, and J.E. Rothman. 2001. A t-SNARE of the endocytic pathway must be activated for fusion. *J. Cell Biol.* 155:961–968. doi:10.1083/jcb.200104092

Pérez-Victoria, F.J., and J.S. Bonifacino. 2009. Dual roles of the mammalian GARP complex in tethering and SNARE complex assembly at the trans-golgi network. *Mol. Cell. Biol.* 29:5251–5263. doi:10.1128/MCB.00495-09

Pérez-Victoria, F.J., G.A. Mardones, and J.S. Bonifacino. 2008. Requirement of the human GARP complex for mannose 6-phosphate-receptor-dependent sorting of cathepsin D to lysosomes. *Mol. Biol. Cell*. 19:2350–2362. doi:10.1091/mbc.E07-11-1189

Pérez-Victoria, F.J., C. Schindler, J.G. Magadán, G.A. Mardones, C. Delevoye, M. Romao, G. Raposo, and J.S. Bonifacino. 2010. Ang2/fat-free is a conserved subunit of the Golgi-associated retrograde protein complex. *Mol. Biol. Cell*. 21:3386–3395. doi:10.1091/mbc.E10-05-0392

Pfeffer, S.R. 1996. Transport vesicle docking: SNAREs and associates. *Annu. Rev. Cell Dev. Biol.* 12:441–461. doi:10.1146/annurev.cellbio.12.1.441

Pfeffer, S.R. 2009. Multiple routes of protein transport from endosomes to the trans Golgi network. *FEBS Lett.* 583:3811–3816. doi:10.1016/j.febslet.2009.10.075

Protopopov, V., B. Govindan, P. Novick, and J.E. Gerst. 1993. Homologs of the synaptobrevin/VAMP family of synaptic vesicle proteins function on the late secretory pathway in *S. cerevisiae*. *Cell*. 74:855–861. doi:10.1016/0092-8674(93)90465-3

Ram, R.J., B. Li, and C.A. Kaiser. 2002. Identification of Sec36p, Sec37p, and Sec38p: components of yeast complex that contains Sec34p and Sec35p. *Mol. Biol. Cell*. 13:1484–1500. doi:10.1091/mbc.01-10-0495

Reaves, B., M. Horn, and G. Banting. 1993. TGN38/41 recycles between the cell surface and the TGN: brefeldin A affects its rate of return to the TGN. *Mol. Biol. Cell*. 4:93–105.

Reddy, P., and M. Krieger. 1989. Isolation and characterization of an extragenic suppressor of the low-density lipoprotein receptor-deficient phenotype of a Chinese hamster ovary cell mutant. *Mol. Cell. Biol.* 9:4799–4806.

Saint-Pol, A., B. Yélamos, M. Amessou, I.G. Mills, M. Dugast, D. Tenza, P. Schu, C. Antony, H.T. McMahon, C. Lamaze, and L. Johannes. 2004. Clathrin adaptor epsinR is required for retrograde sorting on early endosomal membranes. *Dev. Cell*. 6:525–538. doi:10.1016/S1534-5807(04)00100-5

Sannerud, R., J. Saraste, and B. Goud. 2003. Retrograde traffic in the biosynthetic-secretory route: pathways and machinery. *Curr. Opin. Cell Biol.* 15:438–445. doi:10.1016/S0955-0674(03)00077-2

Sapperstein, S.K., D.M. Walter, A.R. Grosvenor, J.E. Heuser, and M.G. Waters. 1995. p115 is a general vesicular transport factor related to the yeast endoplasmic reticulum to Golgi transport factor Uso1p. *Proc. Natl. Acad. Sci. USA*. 92:522–526. doi:10.1073/pnas.92.2.522

Sapperstein, S.K., V.V. Lupashin, H.D. Schmitt, and M.G. Waters. 1996. Assembly of the ER to Golgi SNARE complex requires Uso1p. *J. Cell Biol.* 132:755–767. doi:10.1083/jcb.132.5.755

Shestakova, A., S. Zolov, and V. Lupashin. 2006. COG complex-mediated recycling of Golgi glycosyltransferases is essential for normal protein glycosylation. *Traffic*. 7:191–204. doi:10.1111/j.1600-0854.2005.00376.x

Shestakova, A., E. Suvorova, O. Pavliv, G. Khaidakova, and V. Lupashin. 2007. Interaction of the conserved oligomeric Golgi complex with t-SNARE Syntaxin5a/Sed5 enhances intra-Golgi SNARE complex stability. *J. Cell Biol.* 179:1179–1192. doi:10.1083/jcb.200705145

Smith, R.D., R. Willett, T. Kudlyk, I. Pokrovskaya, A.W. Paton, J.C. Paton, and V.V. Lupashin. 2009. The COG complex, Rab6 and COPI define a novel Golgi retrograde trafficking pathway that is exploited by SubAB toxin. *Traffic*. 10:1502–1517. doi:10.1111/j.1600-0854.2009.00965.x

Spelbrink, R.G., and S.F. Nothwehr. 1999. The yeast GRD20 gene is required for protein sorting in the trans-Golgi network/endosomal system and for polarization of the actin cytoskeleton. *Mol. Biol. Cell*. 10:4263–4281.

Subramaniam, V.N., J. Krijnse-Locker, B.L. Tang, M. Ericsson, A.R. Yusoff, G. Griffiths, and W. Hong. 1995. Monoclonal antibody HFD9 identifies a novel 28 kDa integral membrane protein on the cis-Golgi. *J. Cell Sci.* 108:2405–2414.

Südhof, T.C., and J.E. Rothman. 2009. Membrane fusion: grappling with SNARE and SM proteins. *Science*. 323:474–477. doi:10.1126/science.1161748

Sun, Y., A. Shestakova, L. Hunt, S. Sehgal, V. Lupashin, and B. Storrie. 2007. Rab6 regulates both ZW10/RINT-1 and conserved oligomeric Golgi complex-dependent Golgi trafficking and homeostasis. *Mol. Biol. Cell*. 18:4129–4142. doi:10.1091/mbc.E07-01-0080

Suvorova, E.S., R.C. Kurten, and V.V. Lupashin. 2001. Identification of a human orthologue of Sec34p as a component of the cis-Golgi vesicle tethering machinery. *J. Biol. Chem.* 276:22810–22818. doi:10.1074/jbc.M011624200

Suvorova, E.S., R. Duden, and V.V. Lupashin. 2002. The Sec34/Sec35p complex, a Ypt1p effector required for retrograde intra-Golgi trafficking, interacts with Golgi SNAREs and COPI vesicle coat proteins. *J. Cell Biol.* 157:631–643. doi:10.1083/jcb.200111081

Tai, G., L. Lu, T.L. Wang, B.L. Tang, B. Goud, L. Johannes, and W. Hong. 2004. Participation of the syntaxin 5/Ykt6/GS28/GS15 SNARE complex in transport from the early/recycling endosome to the trans-Golgi network. *Mol. Biol. Cell*. 15:4011–4022. doi:10.1091/mbc.E03-12-0876

Tran, T.H., Q. Zeng, and W. Hong. 2007. VAMP4 cycles from the cell surface to the trans-Golgi network via sorting and recycling endosomes. *J. Cell Sci.* 120:1028–1041. doi:10.1242/jcs.03387

Ungar, D., T. Oka, E.E. Brittle, E. Vasile, V.V. Lupashin, J.E. Chatterton, J.E. Heuser, M. Krieger, and M.G. Waters. 2002. Characterization of a mammalian Golgi-localized protein complex, COG, that is required for normal Golgi morphology and function. *J. Cell Biol.* 157:405–415. doi:10.1083/jcb.200202016

Ungar, D., T. Oka, M. Krieger, and F.M. Hughson. 2006. Retrograde transport on the COG railway. *Trends Cell Biol.* 16:113–120. doi:10.1016/j.tcb.2005.12.004

VanRheenen, S.M., X. Cao, V.V. Lupashin, C. Barlowe, and M.G. Waters. 1998. Sec35p, a novel peripheral membrane protein, is required for ER to Golgi vesicle docking. *J. Cell Biol.* 141:1107–1119. doi:10.1083/jcb.141.5.1107

VanRheenen, S.M., X. Cao, S.K. Sapperstein, E.C. Chiang, V.V. Lupashin, C. Barlowe, and M.G. Waters. 1999. Sec34p, a protein required for vesicle tethering to the yeast Golgi apparatus, is in a complex with Sec35p. *J. Cell Biol.* 147:729–742. doi:10.1083/jcb.147.4.729

Walter, D.M., K.S. Paul, and M.G. Waters. 1998. Purification and characterization of a novel 13 S hetero-oligomeric protein complex that stimulates in vitro Golgi transport. *J. Biol. Chem.* 273:29565–29576. doi:10.1074/jbc.273.45.29565

Wang, Y., G. Tai, L. Lu, L. Johannes, W. Hong, and B.L. Tang. 2005. Trans-Golgi network syntaxin 10 functions distinctly from syntaxins 6 and 16. *Mol. Membr. Biol.* 22:313–325. doi:10.1080/09687860500143829

Wendler, F., and S. Tooze. 2001. Syntaxin 6: the promiscuous behaviour of a SNARE protein. *Traffic*. 2:606–611. doi:10.1034/j.1600-0854.2001.20903.x

Whyte, J.R., and S. Munro. 2001. The Sec34/35 Golgi transport complex is related to the exocyst, defining a family of complexes involved in multiple steps of membrane traffic. *Dev. Cell*. 1:527–537. doi:10.1016/S1534-5807(01)00063-6

Whyte, J.R., and S. Munro. 2002. Vesicle tethering complexes in membrane traffic. *J. Cell Sci.* 115:2627–2637.

Wiederkehr, A., J.O. De Craene, S. Ferro-Novick, and P. Novick. 2004. Functional specialization within a vesicle tethering complex: bypass of a subset of exocyst deletion mutants by Sec1p or Sec4p. *J. Cell Biol.* 167:875–887. doi:10.1083/jcb.200408001

Wu, X., R.A. Steet, O. Bohorov, J. Bakker, J. Newell, M. Krieger, L. Spaapen, S. Kornfeld, and H.H. Freeze. 2004. Mutation of the COG complex subunit gene COG7 causes a lethal congenital disorder. *Nat. Med.* 10:518–523. doi:10.1038/nm1041

Wuestehube, L.J., R. Duden, A. Eun, S. Hamamoto, P. Korn, R. Ram, and R. Schekman. 1996. New mutants of *Saccharomyces cerevisiae* affected in the transport of proteins from the endoplasmic reticulum to the Golgi complex. *Genetics*. 142:393–406.

Yoshino, A., S.R. Setty, C. Poynton, E.L. Whiteman, A. Saint-Pol, C.G. Burd, L. Johannes, E.L. Holzbaur, M. Koval, J.M. McCaffery, and M.S. Marks. 2005. tGolgin-1 (p230, golgin-245) modulates Shiga-toxin transport to the Golgi and Golgi motility towards the microtubule-organizing centre. *J. Cell Sci.* 118:2279–2293. doi:10.1242/jcs.02358

Zeevaert, R., F. Foulquier, J. Jaeken, and G. Matthijs. 2008. Deficiencies in subunits of the Conserved Oligomeric Golgi (COG) complex define a novel group of Congenital Disorders of Glycosylation. *Mol. Genet. Metab.* 93:15–21. doi:10.1016/j.ymgme.2007.08.118

Zeng, Q., T.T. Tran, H.X. Tan, and W. Hong. 2003. The cytoplasmic domain of Vamp4 and Vamp5 is responsible for their correct subcellular targeting: the N-terminal extenSion of VAMP4 contains a dominant autonomous targeting signal for the trans-Golgi network. *J. Biol. Chem.* 278:23046–23054. doi:10.1074/jbc.M303214200

Zolov, S.N., and V.V. Lupashin. 2005. Cog3p depletion blocks vesicle-mediated Golgi retrograde trafficking in HeLa cells. *J. Cell Biol.* 168:747–759. doi:10.1083/jcb.200412003